NASA Contractor Report 187537
ICASE Report No. 91-29

ICASE

DIRECT SIMULATION OF COMPRESSIBLE TURBULENCE IN A SHEAR FLOW

S. Sarkar
G. Erlebacher
M. Y. Hussaini

Contract No. NAS1-18605
March 1991

Institute for Computer Applications in Science and Engineering
NASA Langley Research Center
Hampton, Virginia 23665-5225

Operated by the Universities Space Research Association

National Aeronautics and
Space Administration

Langley Research Center
Hampton, Virginia 23665-5225

DIRECT SIMULATION OF COMPRESSIBLE TURBULENCE IN A SHEAR FLOW[1]

S. Sarkar, G. Erlebacher, and M.Y. Hussaini

Institute for Computer Applications in Science and Engineering

NASA Langley Research Center

Hampton, VA 23665

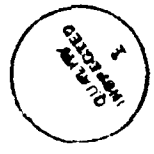

ABSTRACT

The purpose of this study is to investigate compressibility effects on the turbulence in homogeneous shear flow. We find that the growth of the turbulent kinetic energy decreases with increasing Mach number - a phenomenon which is similar to the reduction of turbulent velocity intensities observed in experiments on supersonic free shear layers. An examination of the turbulent energy budget shows that both the compressible dissipation and the pressure-dilatation contribute to the decrease in the growth of kinetic energy. The pressure-dilatation is predominantly negative in homogeneous shear flow, in contrast to its predominantly positive behavior in isotropic turbulence. The different signs of the pressure-dilatation are explained by theoretical consideration of the equations for the pressure variance and density variance. We obtained previously the following results for isotropic turbulence; first, the normalized compressible dissipation is of $O(M_t^2)$, and second, there is approximate equipartition between the kinetic and potential energies associated with the fluctuating compressible mode. Both these results have now been substantiated in the case of homogeneous shear. The dilatation field is significantly more skewed and intermittent than the vorticity field. Strong compressions seem to be more likely than strong expansions.

[1]This research was supported by the National Aeronautics and Space Administration under NASA Contract No. NAS1-18605 while the authors were in residence at the Institute for Computer Applications in Science and Engineering (ICASE), NASA Langley Research Center, Hampton, VA 23665.

1 Introduction

Homogeneous shear flow refers to the problem of spatially homogeneous turbulence sustained by a parallel mean velocity field $\overline{\mathbf{u}} = (Sx_2, 0, 0)$ with a constant shear rate S. Such a flow is perhaps the simplest idealization of turbulent shear flow where there are no boundary effects, and where the given mean flow is unaffected by the Reynolds stresses. Nevertheless, the crucial mechanisms of sustenance of turbulent fluctuations by a mean velocity gradient, and the energy cascade down to the small scales of motion are both present in this flow.

The homogeneous shear flow problem has been studied experimentally by Champagne, Harris and Corrsin (1970), Harris, Graham and Corrsin (1977), and Tavoularis and Corrsin (1981) among others. In these low-speed experiments the statistical properties of the flow do not vary spatially in the transverse (x_2, x_3) plane but they evolve in the streamwise x_1 direction. In theory, the streamwise inhomogeneity can be removed by writing the equations of motion in a reference frame moving with the mean flow $\overline{\mathbf{u}}$. In the moving reference frame, the one-point moments satisfy pure evolution equations in time clearly illustrating that homogeneous turbulence is fundamentally an initial value problem. Rogallo (1981) and Rogers and Moin (1987) have investigated the incompressible homogeneous shear problem at great depth through direct numerical simulations. These simulations, albeit at low turbulence Reynolds numbers, have provided turbulence statistics which are in good agreement with experiments performed at relatively higher Reynolds numbers. Furthermore, since the simulations provide global instantaneous fields, the turbulence can be studied in much greater detail than in physical experiments.

Recently there has been a spurt of activity in the direct numerical simulation (DNS) of three-dimensional compressible turbulence. Decaying isotropic turbulence has been studied by Passot (1987), Erlebacher et al. (1990), Sarkar et al. (1989), and Lee, Lele and Moin (1990). The simulations of Erlebacher et al. (1990) identified different transient regimes including a regime with weak shocks, and also showed that a velocity field which is initially solenoidal can develop a significant dilatational component at later times. Sarkar et al. (1989) investigated the statistical moments associated with the compressible mode in their

simulations, and determined a quasi-equilibrium in these statistics for moderate turbulent Mach numbers which was then used to model various dilatational correlations. Lee, Lele and Moin (1990) studied eddy shocklets which developed in their simulations when the initial turbulent Mach number was sufficiently high ($M_t > 0.6$). Kida and Orszag (1990) primarily studied power spectra, and energy transfer mechanisms between the solenoidal and dilatational components of the velocity in their simulations of forced isotropic turbulence.

Physical experiments have not been and perhaps cannot be performed for homogeneous shear flows at flow speeds which are sufficiently high to introduce compressible effects on the turbulence. However, direct numerical simulation of this problem could provide meaningful data, especially since DNS for the incompressible problem has been successful in giving realistic flow fields. The compressible problem was considered by Feiereisen et al. (1982) who performed relatively low resolution 64^3 simulations and concluded that compressibility effects are small. Recently Blaisdell (1990) has also considered compressible shear flow. We have performed both 96^3 and 128^3 simulations which have allowed us to obtain some interesting new results regarding the influence of compressibility on the turbulence. In contrast to the results of Feiereisen et al., our simulations which start with incompressible initial data develop significant rms levels of dilatational velocity and density. We find that the growth rate of the kinetic energy decreases with increasing Mach number as well as increasing rms density fluctuations and show that the compressible dissipation and pressure-dilatation contribute to this effect. Apart from rms levels of the fluctuating variables, we have also examined their probability density functions (pdf) and higher order moments. The dilatational field has different skewness and flatness characteristics relative to the vorticity field. In particular, the dilatational field has a significant negative skewness and is more intermittent than the vorticity field.

2 Simulation Method

The compressible Navier-Stokes equations are written in a frame of reference moving with the mean flow $\bar{u}_1$. This transformation, which was introduced by Rogallo (1981) for incompress-

ible homogeneous shear, removes the explicit dependence on $\overline{u}(x_2)$ in the exact equations for the fluctuating velocity, thus allowing the imposition of periodic boundary conditions in the x_2 direction. The relation between x_i^* and the lab frame x_i is

$$x_1^* = x_1 - Stx_2 \quad , \quad x_2^* = x_2 \quad , \quad x_3^* = x_3$$

Here S denotes the constant shear rate $\bar{u}_{1,2}$. In the transformed frame x_i^*, the compressible Navier-Stokes equations take the following form

$$\partial_t \rho + (\rho u_i')_{,i} - St(\rho u_2')_{,1} = 0 \tag{1}$$

$$\begin{aligned} \partial_t(\rho u_i') + (\rho u_j' u_i')_{,j} &= -p_{,i} + \tau'_{ij,j} - S\rho u_2' \delta_{i1} \\ &+ St(\rho u_2' u_i')_{,1} + Stp_{,1}\delta_{i2} - St\tau'_{i2,1} \end{aligned} \tag{2}$$

$$\begin{aligned} \partial_t p + u_j' p_{,j} + \gamma p u'_{j,j} &= Stu_2' p_{,1} + \gamma Stp u'_{2,1} \\ &+ (\gamma - 1)\kappa[T_{,jj} - 2StT_{,12} + S^2t^2T_{,11}] + \Phi \end{aligned} \tag{3}$$

$$p = \rho RT \tag{4}$$

where $\Phi = \tau_{ij}u_{i,j}$ is the dissipation function, u_i' the fluctuating velocity, ρ the instantaneous density, p the pressure, T the temperature, R the gas constant, and κ the thermal conductivity. The viscous stress is

$$\tau_{ij} = \mu(u_{i,j} + u_{j,i}) - \frac{2}{3}\mu(u_{k,k})\delta_{ij}$$

where μ is the molecular viscosity which is taken to be constant. All the derivatives in the above system are evaluated with respect to the transformed coordinates x_i^*.

Since Eqs. (1)-(4) do not have any explicit dependence on the spatial coordinates x_i^*, and because the homogeneous shear flow problem, by definition, does not have any boundary effects, periodic boundary conditions are allowable on all the faces of the computational box. Of course, in order to obtain realistic turbulence fields it is necessary that the length of the

computational domain be much larger than the integral length scale of the turbulence. Spectral accuracy is obtained by using a Fourier collocation method for the spatial discretization of the governing equations. FFT's are used to obtain the Fourier representation from the data in physical space and thereby calculate derivatives. In order to avoid expensive evaluations of convolutions in Fourier space, the nonlinear terms are directly evaluated in physical space as products of derivatives. It has been shown by Canuto, Hussaini, Quarteroni and Zang (1988), that the ensuing aliasing error is negligible if the significant spatial scales of the computed variable are resolved on the grid. A third order, low storage Runge-Kutta scheme is used for advancing the solution in time.

The computational mesh becomes progressively skewed because the mean flow velocity $\bar{u}_1$ with which the mesh moves has a variation in the x_2 direction. In order to control the loss of accuracy caused by excessive skewness of the mesh, we interpolate the solution on the grid at $St = 0.5$ shown in Fig. 2a, onto the grid sketched in Fig. 2b which is skewed in the opposite direction and corresponds to $St = -0.5$. Since the solution is periodic, the interpolation is straightforward in physical space. However, the remesh procedure introduces spectral aliasing errors as pointed out by Rogallo (1981). In the dealiasing procedure used here, the higher Fourier modes are truncated both before and after the remesh.

Initial conditions have to be prescribed for u_i', ρ, p and T. The initial velocity field is split into two independent components, that is, $u_i' = u_i^{I'} + u_i^{C'}$, each component having a zero average. The solenoidal velocity field $u_i^{I'}$ which satisfies $\nabla.\mathbf{u}^{I'} = 0$ is chosen to be a random Gaussian field with the power spectrum

$$E(k) = k^4 \exp(-2k^2/k_m^2) \tag{5}$$

where k_m denotes the wave number corresponding to the peak of the power spectrum. The compressible velocity $u_i^{C'}$ which satisfies $\nabla \times \mathbf{u}^{C'} = 0$ is also chosen to be a random Gaussian field satisfying the same power spectrum, Eq. (5). The power spectra of the two velocity components are scaled so as to obtain a prescribed $u_{\rm rms} = \sqrt{\overline{u_i' u_i'}}$, and a prescribed $\chi =$

$u^C_{\rm rms}/u_{\rm rms}$ which is the compressible fraction of kinetic energy. The pressure $p^{I'}$ associated with the incompressible velocity is evaluated from the Poisson equation

$$\nabla^2 p^{I'} = -2\overline{\rho} S u^{I'}_{2,1} - \overline{\rho} u^{I'}_{i,j} u^{I'}_{j,i} \tag{6}$$

It remains to specify the thermodynamic variables. The mean density $\overline{\rho}$ is chosen equal to unity, and $\overline{p}$ is chosen so as to obtain a prescribed Mach number $u_{\rm rms}/\sqrt{\gamma\overline{p}/\overline{\rho}}$ characterizing the turbulence. The fluctuating density ρ' and compressible pressure $p^{C'}$ are chosen as random fields with the power spectrum Eq. (5) and prescribed $\rho_{\rm rms}$ and $p^C_{\rm rms}$. The pressure then becomes $p = \overline{p} + p^{I'} + p^{C'}$, the density is $\rho = \overline{\rho} + \rho'$, and the temperature T is obtained from the equation of state $p = \rho RT$.

3 Results

We have performed simulations for a variety of initial conditions and obtained turbulent fields with Taylor microscale Reynolds numbers Re_λ up to 35 and turbulent Mach numbers M_t up to 0.6. Note that $Re_\lambda = q\lambda/\nu$ where $q = \sqrt{\overline{u'_i u'_i}}$ and $\lambda = q/\sqrt{\overline{\omega'_i \omega'_i}}$, while $M_t = q/\overline{c}$ where $\overline{c}$ is the mean speed of sound. The computational domain is a cube with side 2π. The results discussed here were obtained with a uniform 96^3 mesh overlaying the computational domain. The initial values of some of the important non-dimensional parameters associated with the DNS cases ranged as follows: $3.6 < (SK/\epsilon)_0 < 7.2$, $16 < Re_{\lambda,0} < 24$, $0.2 < M_{t,0} < 0.4$, and $0 < \chi < 0.15$. We note that K denotes the turbulent kinetic energy and ϵ the turbulent dissipation rate.

In previous work by Erlebacher et al. (1990) on isotropic turbulence, it was found that for a given initial Re_λ, the initial choice of the non-dimensional quantities M_t, $\rho_{\rm rms}/\overline{\rho}$, $T_{\rm rms}/\overline{T}$, $p_{\rm rms}/\overline{p}$ and χ had a strong and lasting influence on the temporal evolution of the turbulence. The different choices of initial conditions that lead to different regimes were classified by Erlebacher et al. Even though the long time statistics in isotropic turbulence are, in general, strongly dependent on the initial conditions, there is a quantity in isotropic turbulence which

has a large degree of universality (in the absence of shocks). This quantity is the partition factor F defined by

$$F = \gamma^2 M_t^2 \chi / \overline{p_C'^2} \tag{7}$$

which was shown by Sarkar et al. (1989) to equal unity (to lowest order) in a low M_t asymptotic analysis, and to approach unity from a variety of initial conditions in direct simulations of isotropic turbulence with M_t up to 0.6. The physical interpretation of $F \rightarrow 1$ is that there is a tendency towards equipartition between the kinetic energy and potential energy of the compressible component of the turbulence.

In the case of initially isotropic turbulence subjected to homogeneous shear, for a given initial energy spectrum, the solution of the incompressible equations depends on the initial conditions through the parameters $(SK/\epsilon)_0$ and $Re_{\lambda,0}$. The compressible case depends additionally on the initial levels of the thermodynamic fluctuations, dilatational velocity component and turbulent Mach number. Apart from the influence of initial conditions, another and perhaps more important feature is the influence of local compressibility and interactions between the velocity and thermodynamic fields on the statistics at a given time. Equilibrium scalings (if present) are also important to ascertain so as to improve the present capabilities of modeling compressible turbulence. In order to address these issues, we present selected results on second-order moments, pdf's (probability density functions), and higher-order moments of both the velocity and thermodynamic fields.

3.1 Second-order moments

Evidence from physical and numerical experiments (e.g., Tavoularis and Corrsin (1981) and Rogallo (1981)) indicate that for incompressible homogeneous shear, both the turbulent kinetic energy and the turbulent dissipation rate increase exponentially. Though our simulations are in accord with this picture of exponential growth, we note that Bernard and Speziale (1990) have recently proposed an alternative picture where, after a substantially long period of exponential growth, the turbulent energy eventually becomes bounded for large St through a saturation induced by vortex stretching. In order to explore the effect

of initial levels of compressibility on the evolution of the turbulent statistics, we have performed simulations based on two distinct types of initial conditions. The simulations of the first type, whose results are shown in Figs. 3a-6a, start with incompressible data, that is, $\rho_{\rm rms,0} = \chi_0 = 0$, but have different initial Mach numbers $M_{t,0}$. The second type of simulations, whose results are shown in Fig. 3b-6b, start with different levels of initial rms density fluctuations $r_{\rho,0} = (\rho_{\rm rms}/\overline{\rho})_0$ and compressible fraction of kinetic energy χ_0, but have the same $M_{t,0} = 0.3$. We note that all the cases of Figs. 3-6 have $Re_{\lambda,0} = 24$ and $(SK/\epsilon)_0 = 7.2$. The DNS results of Fig. 3a show that the level of the Favre-averaged kinetic energy K at a given time decreases with increasing $M_{t,0}$ in the simulations with the first type of initial conditions, while Fig. 3b shows that the level of K also decreases with increasing χ_0 and $r_{\rho,0}$ for the simulations with the second type of initial conditions. Thus an increase in compressibility level, either due to increased Mach number or increased dilatational fraction of the velocity field *decreases* the growth of turbulent kinetic energy in the case of homogeneous shear flow. Fig. 4 shows that the development of the turbulent dissipation ϵ has two phases. In the first phase ($St < 4$) the higher compressibility cases have higher values of ϵ probably due to the buildup of the compressible dissipation ϵ_c. Later, in the second phase, the trend reverses and the compressible cases have lower ϵ relative to the incompressible case. Thus, compressibility results in decreased growth of both ϵ and K.

In order to explain the phenomenon of reduced growth rate of kinetic energy, we consider the equation governing the kinetic energy of turbulence in homogeneous shear which is

$$\frac{d}{dt}(\overline{\rho}K) = -S\overline{\rho}\widetilde{u_1''u_2''} - \overline{\rho}\epsilon + \overline{p'd'} \tag{8}$$

where $\overline{\rho}\epsilon$ is the turbulent dissipation rate and $\overline{p'd'}$ is the pressure-dilatation. The overbar over a variable denotes a conventional Reynolds average, while the overtilde denotes a Favre average. A single superscript $'$ represents fluctuations with respect to the Reynolds average, while a double superscript $''$ signifies fluctuations with respect to the Favre average. It was shown in Sarkar et al. (1989) that the effect of compressibility on the dissipation rate can

be advantageously studied by using the decomposition

$$\epsilon = \epsilon_s + \epsilon_c \tag{9}$$

where the solenoidal dissipation rate $\epsilon_s = \overline{\nu\omega_i'\omega_i'}$ and the compressible dissipation rate $\epsilon_c = (4/3)\overline{\nu d'^2}$. Here ω_i' denotes the fluctuating vorticity and d' denotes the fluctuating divergence of velocity. We note that the correlations involving the fluctuating viscosity have been neglected on the rhs of Eq. (9). Substituting Eq.(9) into Eq.(8) gives

$$\frac{d}{dt}(\overline{\rho}K) = -S\overline{\rho}\widetilde{u_1''u_2''} - \overline{\rho}\epsilon_s - \overline{\rho}\epsilon_c + \overline{p'd'} \tag{10}$$

and the last two terms represent the explicit influence of the non-solenoidal nature of the fluctuating velocity field in the kinetic energy budget. The DNS time histories for ϵ_c and $\overline{p'd'}$ are presented in Figs. 5-6 respectively. The compressible dissipation ϵ_c is always positive (as expected) and when starting from a zero initial value as in Fig. 5a shows a monotonic increase with time. The pressure-dilatation $\overline{p'd'}$ is highly oscillatory as seen in Fig. 6. Though $\overline{p'd'}$ can be both positive or negative it tends to be predominantly negative. The tendency of $\overline{p'd'}$ to be negative in homogeneous shear is clearly shown in Fig. 7 where the oscillations are smoothed out by plotting values of $\overline{p'd'}$ obtained by averaging over successive time intervals. Interestingly enough, on comparing Figs. 5a and 7a it seems that the time averaged values of $-\overline{p'd'}$ and ϵ_c are of the same order and exhibit similar trends of increase with St and $M_{t,0}$. These DNS results along with the kinetic energy equation (10) show that both ϵ_c and $\overline{p'd'}$ have a dissipative effect on the turbulent kinetic energy.

The predominantly negative values of $\overline{p'd'}$ in homogeneous shear is in contrast to the predominantly positive values reported in Sarkar et al. (1989) for the case of decaying isotropic turbulence. To understand this contrasting behavior of $\overline{p'd'}$ we write the exact equation for the pressure variance which is applicable to both these flows

$$\frac{d}{dt}\overline{p'^2} = -2\gamma\overline{p}\,\overline{p'd'} - (2\gamma - 1)\overline{p'p'd'} - 2\epsilon_p + \phi_p \tag{11}$$

where ϕ_p is a term depending on mean viscosity and mean conductivity which is negligible compared to ϵ_p. Here $\epsilon_p = (\gamma - 1)R\overline{\kappa}\,\overline{\rho T_{,j}'T_{,j}'}$ and can be called the pressure dissipation

term by virtue of being a sink on the rhs of Eq. (11). Comparing Eq. (10) and Eq. (11) it is clear that $\overline{p'd'}$ acts to transfer energy between the kinetic energy of turbulence $\bar{\rho}K$ and the potential energy of the turbulence $\overline{p'^2}/(2\gamma\bar{p})$. In the case of homogeneous shear the rms values of the velocity and pressure increase with time. Now, the third term on the rhs of Eq. (11) is always negative and therefore a sink for the pressure variance. For small $p'/\bar{p}$ we can neglect the second term on the rhs of Eq. (11) with respect to the first term. Therefore for $\overline{p'^2}$ to *increase* with time, a source term is necessary which implies that $\overline{p'd'}$ be *negative* in accord with the DNS results. We note that a similar analysis of the equations for $\overline{\rho'^2}$ and $\overline{T'^2}$ indicate that $\overline{\rho'd'}$ and $\overline{T'd'}$ also have to be predominantly negative in this flow.

In decaying isotropic turbulence $\overline{p'^2}$ has to decay with time; however, because ϵ_p is sufficient to ensure decay of $\overline{p'^2}$ the sign of $\overline{p'd'}$ cannot be determined from Eq. (11). Alternatively, we consider the exact density variance equation which for homogeneous shear flow is

$$\frac{d}{dt}\overline{\rho'^2} = -2\bar{\rho}\overline{\rho'd'} - \overline{\rho'\rho'd'} \tag{12}$$

For small $\rho'/\bar{\rho}$, the first term on the rhs of Eq. (11) dominates the second term. Therefore for $\overline{\rho'^2}$ to decrease with time it is necessary that $\overline{\rho'd'}$ be predominantly positive. If we assume that the thermodynamic fluctuations are approximately isentropic in this case (DNS supports this assumption), it immediately follows that $\overline{p'd'}$ is also predominantly positive in decaying isotropic turbulence. Thus, the role of $\overline{p'd'}$ as a mechanism for energy transfer between the kinetic energy and potential energy dictates its differing signs in homogeneous shear and unforced isotropic turbulence.

Fig. 8a shows the temporal evolution of M_t for different choices of the initial values for M_t and Re_λ. For all the cases, the turbulent Mach number shows a monotonic increase with time for the range of St spanned by the simulations. Two results of the analysis of Sarkar et al. (1989) which were validated previously in isotropic turbulence are now checked in homogeneous shear flow. These results are, first, the compressible dissipation obeys the scaling $\epsilon_c/\epsilon_s = \alpha M_t^2$, and second, the partition factor $F \simeq 1$ (see Eq. (7) for the definition of F) which implies a tendency toward equipartition between the kinetic and potential energies

of the fluctuating compressible mode. Fig. 9a shows that for a variety of DNS cases the ratio $\epsilon_c/(\epsilon_s M_t^2)$ approaches an equilibrium value of approximately 0.5 for large enough St. The same ratio is plotted as a function of local M_t in Fig. 9b. Thus Fig. 9 supports our previously derived result on the dependence of the compressible dissipation on turbulent Mach number. Zeman (1989) had proposed the scaling $\epsilon_c/\epsilon_s = 1 - \exp\{[(M_t - 0.1)/0.6]^2\}$ which is clearly in contradiction with the DNS results of Fig. 9. The partition factor F is seen in Fig. 10a to approach and oscillate around an equilibrium value of approximately 0.95 indicating that equipartition in the energies associated with the compressible mode holds in the case of homogeneous shear too. In Fig. 10b we show the behavior of $F_T = \gamma^2 M_t^2 \chi/\overline{p'^2}$ which is defined using the total pressure variance rather than the compressible pressure variance appearing in the definition of F. The parameter F_T also appears to reach values independent of initial conditions, however this trend is less pronounced in F_T relative to F.

In Fig. 11 we show the time evolution of rms density and temperature fluctuations. It appears that both the rms normalized density and temperature fluctuations eventually scale as M_t^2. The rms pressure also scales as M_t^2. Erlebacher et al. (1990) decomposed the pressure p into an incompressible component p^I and a compressible component p^C. The behavior of $p^C_{\rm rms}$ and $p^I_{\rm rms}$ is shown in Fig. 12. The instantaneous incompressible pressure $p^{I'}$ satisfies the Poisson equation Eq. (6). The compressible pressure $p^{C'} = p' - p^{I'}$ is the remaining part of the pressure which arises from both density variations and non-zero divergence of the velocity. Fig. 12 indicates that the rms of both components of the normalized pressure vary like M_t^2. A simple order of magnitude analysis of Eq. (6) along with recognition of the fact that $SK/\epsilon = O(1)$ shows that $p^I_{rms}/\overline{p} = O(M_t^2)$. Thus it seems that in homogeneous shear the conventionally accepted Mach number variation holds for $p^I_{\rm rms}$, $p^C_{\rm rms}$ and $p_{\rm rms}$.

The evolution of $p^{C'}$ in the case where the initial data is incompressible can be understood by considering the following equation for compressible pressure (see Erlebacher et al. (1990) for details) where heat conduction and viscous effects have been neglected

$$\partial_t p^{C'} + u_i^{I'} p^{C'}_{,i} + u_i^{C'} p^{C'}_{,i} + u_i^{C'} p^{I'}_{,i} + \gamma(1 + p^{C'}) u^{C'}_{i,i} = -(\partial_t p^{I'} + u_i^{I'} p^{I'}_{,i}) \qquad (13)$$

Since $p^{C\prime}$ and $u_i^{C\prime}$ are initially zero the growth of $p^{C\prime}$ is due to the forcing by the incompressible pressure on the rhs of Eq. (13). This forcing causes $p^C_{\rm rms}/\overline{p}$ to become $O(p^I_{\rm rms}/\overline{p}) = O(M_t^2)$ on the convective time scale which explains the trend seen in the three lower curves of Fig. 12b. The top curve of Fig. 12b, which corresponds to a case with initially non-zero $p^C_{\rm rms}$ and $u^C_{\rm rms}$, also shows the same trend indicating that the forcing by the incompressible velocity field (through p^I) has a substantial influence in determining the level of $p^C_{\rm rms}$.

3.2 Probability density functions and higher order moments

The probability density function (pdf) gives a comprehensive description of a fluctuating variable because it formally enables the calculation of all the statistical moments. Second-order moments (discussed in the previous section) are probably the most important statistical indicators of the turbulence because they characterize intensities and cross-correlations of the fluctuating variables. Higher-order moments such as the skewness and flatness give additional information on the statistical distribution of the variable, for example, a positive skewness indicates a pdf which is skewed towards positive fluctuations from the mean, while a large flatness indicates a large propensity for the occurrence of extreme values of the variable. The skewness $Sk(\theta)$ and flatness $Fl(\theta)$ of a variable θ are defined by

$$Sk(\theta) = \frac{\overline{\theta'^3}}{(\overline{\theta'^2})^{3/2}}$$

$$Fl(\theta) = \frac{\overline{\theta'^4}}{(\overline{\theta'^2})^2}$$

A quantity with a Gaussian pdf has $Sk = 0$ and $Fl = 3$. In this section, we present results on pdf, skewness and flatness of some variables for a DNS case with significant compressibility levels. The initial nondimensional parameters for this case are

$$Re_\lambda = 24 \quad , \quad SK/\epsilon = 7.2 \quad , \quad M_t = 0.4 \quad , \quad \chi = 0 \quad , \quad \rho_{\rm rms}/\overline{\rho} = 0 \quad , \quad p^C_{\rm rms}/\overline{p} = 0$$

The pdf f_u of the streamwise fluctuating velocity in Fig. 13a appears to be symmetric around the origin. The skewness and flatness of u have insignificant deviations from Gaussian

values. The experiments of Tavoularis and Corrsin (1981) in homogeneous shear flow and Frenkiel and Klebanoff (1973) in the log-region of the flat plate turbulent boundary layer also indicate that u is approximately Gaussian. The pdf's of the other components of the velocity are very similar to those of the streamwise velocity component. However the transverse velocity v develops a somewhat higher flatness ($Fl(v) = 3.3$ at $St = 8$) than the other velocity components. Fig. 13b shows the pdf f_M of the Mach number $M = q/c$ where q is the instantaneous flow speed and c is the instantaneous speed of sound. M has maximum values of 1.7 and 3.2 at $St = 1$ and $St = 8$ respectively, indicating that the pdf of M has exceptionally long tails.

We now investigate quantities related to the velocity derivatives. Figs. 14a-b show the pdfs of the spanwise vorticity component ω_z and the dilatation d. Both pdfs are skewed towards negative values. Higher-order moments of the vorticity components and dilatation are shown in Fig. 15. The skewness of the dilatation (see Fig. 15a) reaches values of about -0.5, signifying that local compressions are more likely than local expansions in the flow. Because of the invariance of the homogeneous shear problem to a reflection of the spanwise (z direction) axis, the ω_x and ω_y components have zero skewness. The dilatational field has larger flatness than the vorticity field, indicating that it is more intermittent than the vorticity field.

In this DNS case, the maximum magnitude of dilatation in the compression regions attains values which are about an order of magnitude larger than the rms dilatation. Lee, Lele and Moin (1990) have also observed such high values of the maximum dilatation in isotropic turbulence, and have furthermore associated these high values with dynamically significant eddy shocklets. However, in order to assess the importance of these high dilatation regions it is necessary not only to identify the magnitude of the maximum dilatation but also to calculate the contribution of these regions to the rms dilatation. We find that, at $St = 8$, the compressive regions with a magnitude of dilatation larger than 3 times the rms dilatation contribute only about 2% to the variance of dilatation. This suggests that shocklet

dissipation is not the dominant contributory mechanism to the compressible dissipation for $M_t < 0.5$.

From Fig. 16a it appears that the imposition of shear does not alter the skewness and flatness of the Mach number M appreciably from the isotropic turbulence values at $St = 0$. The fact that M is bounded from below and not from above may be responsible for the departure of skewness and flatness from Gaussian values. The instantaneous values of M can become rather large (the ratio $M_{\max}/M_t = 5.8$ at $St = 8$), but the flatness level of 4 at $St = 8$ indicates that these large extrema have a relatively low probability of occurrence. The long tail in the pdf of M (see Fig. 13b and the previous discussion of the figure) does not seem to contribute significantly at the level of third and fourth moments. Fig. 16b shows that the velocity field can be highly supersonic ($M_{\max} = 3.3$ at $St = 8$). Though the percentage of the volume occupied by supersonic fluctuations, denoted by ϕ_{super} in Fig. 16b, increases with time, its maximum value is a modest 4.9% at $St = 8$.

4 Characteristics of the instantaneous flow

The previous sections have focused on the influence of compressibility on the statistical attributes of homogeneous shear turbulence. We now present some preliminary results on the spatial characteristics of the instantaneous turbulence from ongoing flow visualization. Figs. 17-20 are results from the flow field at $St = 9$ for a case which has the following initial nondimensional parameters

$$Re_\lambda = 21 \quad , \quad SK/\epsilon = 5.8 \quad , \quad M_t = 0.3 \quad , \quad \chi = 0.09 \quad , \quad \rho_{\text{rms}}/\overline{\rho} = 0.09 \quad , \quad p^C_{\text{rms}}/\overline{p} = 0.13$$

By $St = 9$ the initially isotropic turbulence develops into a realistic representation of homogeneous shear turbulence. The turbulence at $St = 9$ has $M_t = 0.42$, $\rho_{\text{rms}}/\overline{\rho} = 0.12$ and $\chi = 0.06$, which implies a moderate level of compressibility, and has a $Re_\lambda = 32$. One of the important characteristics of the velocity field is the extent and topology of supersonic regions. Fig. 17 shows a 3-D contour plot of regions with fluctuating Mach number $M > 1$. These regions of supersonic fluctuations are small discrete regions scattered through the flow

domain, and are elongated in the streamwise direction. The volume occupied by the regions with supersonic fluctuations is small. Fig. 18 shows the dilatation $\nabla.\mathbf{u}'$ in a plane parallel to the (x_1, x_2) plane. The regions in black are expansion regions with positive dilatation, while the regions in grey and white are compression regions with negative dilatation. Both the compression regions and the expansion regions are very elongated in the streamwise x_1 direction. The white portions in the dilatation plot of Fig. 18 correspond to compression regions where the magnitude of dilatation is larger than the maximum positive dilatation. The magnitude of dilatation in these white regions are up to 50% larger than the maximum positive dilatation indicating that compressions are stronger than the expansions. As Fig. 18 shows, the white regions of strong compression are small and discrete elements which occupy a small portion of the plane. Figs. 19a and 19b are contour plots of the magnitude of $u_i^{I'}$ and $u_i^{C'}$ respectively in a plane parallel to the (x_1, x_2) plane. Regions with large gradients seem to be more prevalent in the $u_i^{C'}$ field relative to the $u_i^{I'}$ field. Figs. 20a and 20b show the incompressible pressure $p^{I'}$ and the compressible pressure $p^{C'}$ in the same plane considered in Fig. 19. It is clear that the $p^{I'}$ field has significant differences with respect to the $p^{C'}$ field. The compressible pressure has higher gradients and more pronounced small scale features than the incompressible pressure. Elongated and inclined structures are also visible in the $p^{C'}$ field.

5 Conclusions

We have performed direct numerical simulations of homogeneous shear flow using a spectral collocation technique and analyzed the data base in order to quantify compressibility effects on the turbulence. An increase in the compressibility level (i.e. turbulent Mach number, density fluctuations or rms dilatational velocity fluctuations) leads to a decrease in the growth of turbulent kinetic energy. In the compressible case, the kinetic energy equation has two additional terms, the compressible dissipation and the pressure-dilatation. Both these terms have a dissipative contribution in shear flow, leading to the reduced growth of the turbulent kinetic energy. The $O(M_t^2)$ variation of the compressible dissipation which

was obtained previously by an asymptotic theory and then verified in the DNS of isotropic turbulence, has now been substantiated by the DNS of homogeneous shear turbulence. The pressure-dilatation is a more difficult term to characterize, because it can be either positive or negative and also because gradient transport arguments are clearly inapplicable. Our DNS show that the pressure-dilatation is predominantly negative in the homogeneous shear case in contrast to its predominantly positive character in decaying isotropic turbulence. Analysis shows that, in the transport equation for the pressure variance, the pressure-dilatation has to be a source in the case of homogeneous shear (where the turbulence grows) and a sink in the case of decaying isotropic turbulence, thus accounting for the opposite signs of the pressure-dilatation in the two flows. In the core region of inhomogeneous aerodynamic flows, perhaps the pressure-dilatation is predominantly negative so as to transfer energy from the velocity field to the pressure field.

It is well known that, for low-speed flows, the rms pressure normalized by the mean pressure varies as $O(M_t^2)$. Our DNS results support this scaling of the rms of pressure, density and temperature fluctuations for compressible homogeneous shear flow. These DNS results and our analysis suggest that such a scaling may be valid for those inhomogeneous flows where the thermodynamic fluctuations arise due to high-speed effects and not due to other factors such as external heating or cooling, and mixing of fluids with different densities or temperatures. We have studied the probability density functions and higher-order moments of the dilatation and the vorticity. The dilatation field has appreciable negative skewness indicating a preponderance of compressions over expansions, and has a larger flatness than the vorticity indicating that it is more intermittent than the vorticity. The intermittent regions of negative dilatation were found to have only a small contribution to the compressible dissipation for $M_t < 0.5$.

Acknowledgements

On the occasion of John Lumley's 60th birthday, SS is pleased to thank John for teaching him turbulence and motivating him to pursue research in the field of turbulence. The authors

wish to thank Tom Gatski and Charles Speziale for their comments on a preliminary draft of this manuscript, and Tom Zang for helpful discussions.

References

Bernard, P.S., and Speziale, C. G. (1990) Bounded Energy States in Homogeneous Turbulent Shear Flow - An Alternative View. *ICASE Report No. 90-66*, submitted to Phys. Fluids A.

Blaisdell, G.A., Reynolds, W.C., Mansour, N.N., Zeman, O., and Aupoix, B. (1990) Growth of Turbulent Kinetic Energy in Compressible Homogeneous Turbulent Shear Flow. *43rd Annual Meeting of the APS/Division of Fluid Dynamics*, Cornell University, N.Y. (November 1990).

Canuto, C., Hussaini, M.Y., Quarteroni, A., and Zang, T.A. (1988) *Spectral Methods in Fluid Dynamics.* Springer-Verlag, Berlin.

Champagne, F.H., Harris, V.G., and Corrsin, S. (1970). Experiments on Nearly Homogeneous Turbulent Shear Flow. *J. Fluid Mech.*, **41**, 81.

Erlebacher, G., Hussaini, M.Y., Kreiss, H.O., and Sarkar, S. (1990) The Analysis and Simulation of Compressible Turbulence. *Theoret. Comput. Fluid Dynamics*, **2**, 73.

Feiereisen, W.J., Shirani, E., Ferziger, J.H., and Reynolds, W.C. (1982) Direct Simulation of Homogeneous Turbulent Shear Flows on the Illiac IV Computer: Applications to Compressible and Incompressible Modelling. In *Turbulent Shear Flows 3*, pp. 309-319. Springer-Verlag, Berlin.

Frenkiel, F.N., and Klebanoff, P.S. (1973) Probability Distributions and Correlations in a Turbulent Boundary Layer. *Phys. Fluids*, **16**, 725.

Harris, V.G., Graham, J.A.H., and Corrsin, S. (1977). Further Experiments in Nearly Homogeneous Turbulent Shear Flow. *J. Fluid Mech.*, **81**, 657.

Kida, S. and Oszag, S.A. (1990). Energy and Spectral Dynamics in Forced Compressible Turbulence. Submitted to *J. Fluid Mech.*

Lee, S., Lele, S.K., and Moin, P. (1990) Eddy-shocklets in Decaying Compressible Turbulence. *CTR Manuscript 117.*

Passot, T. (1987). Simulations numeriques d'ecoulements compressibles homogenes en regime turbulent : application aux nuages moleculaires. *Ph. D. Thesis, University of Paris.*

Rogallo, R.S. (1981). Numerical Experiments in Homogeneous Turbulence. *NASA TM 81315.*

Rogers, M.M., and Moin, P. (1987). The Structure of the Vorticity Field in Homogeneous Turbulent Flows. *J. Fluid Mech.*, **176**, 33.

Sarkar, S., Erlebacher, G., Hussaini, M.Y., and Kreiss, H.O. (1989) The Analysis and Modeling of Dilatational Terms in Compressible Turbulence. *ICASE Report No. 89-79, J. Fluid Mech* (in press).

Tavoularis, S., and Corrsin, S. (1981). Experiments in Nearly Homogeneous Turbulent Shear Flow with a Uniform Mean Temperature Gradient. *J. Fluid Mech.*, **104**, 311.

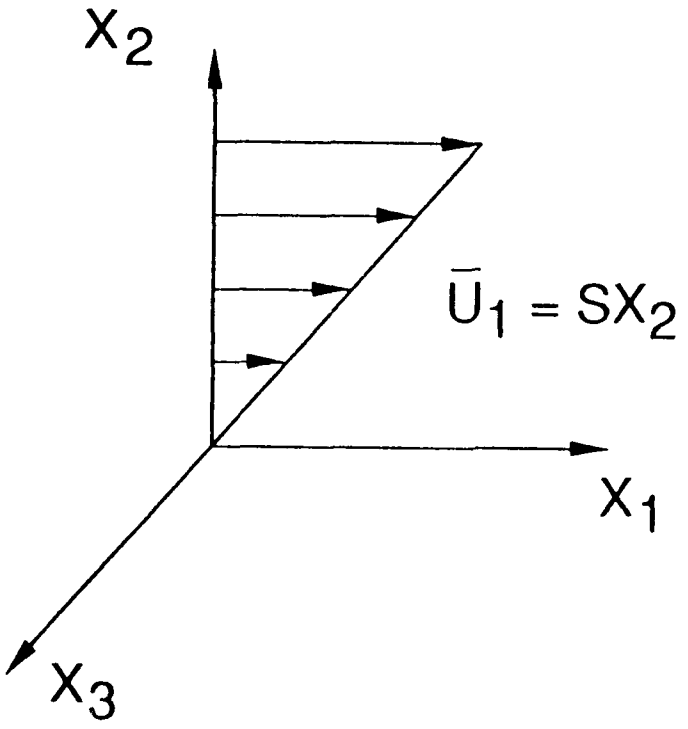

Figure 1 Schematic of homogeneous shear flow.

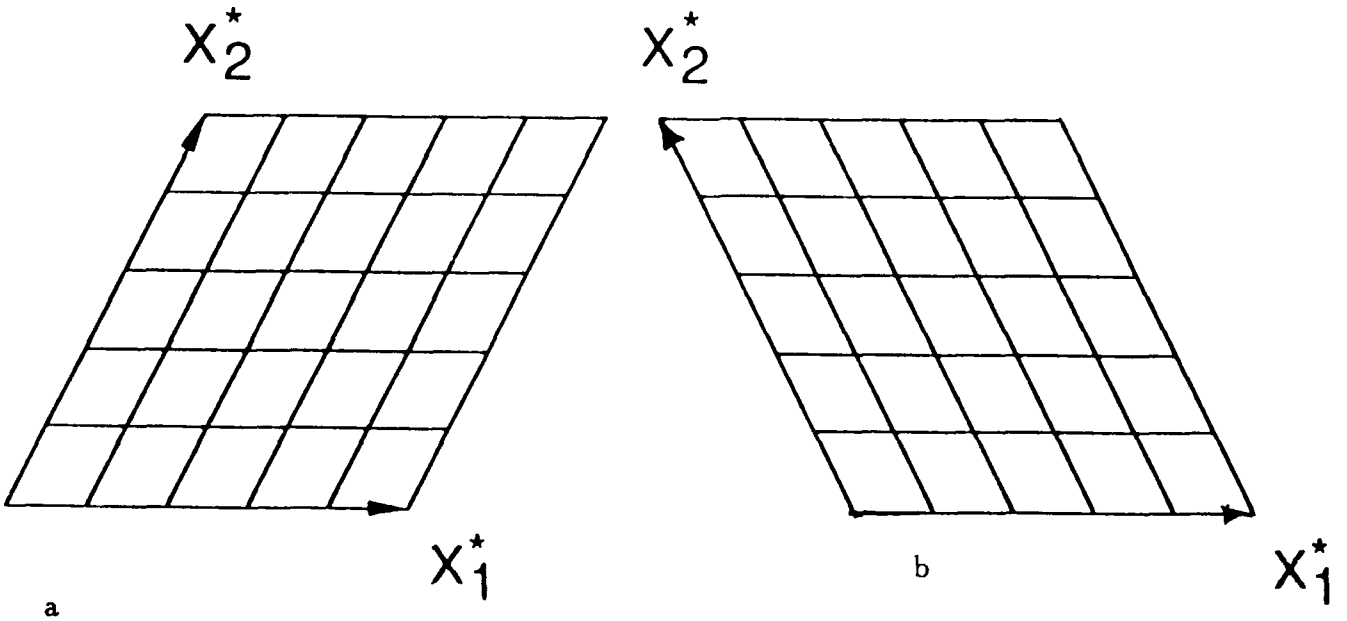

Figure 2 Schematic of regrid procedure.

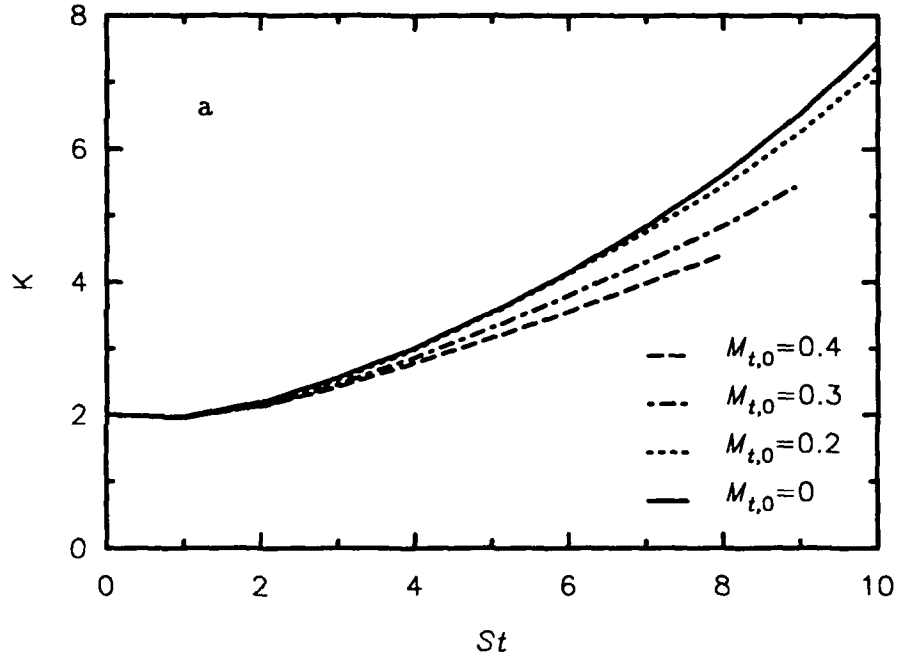

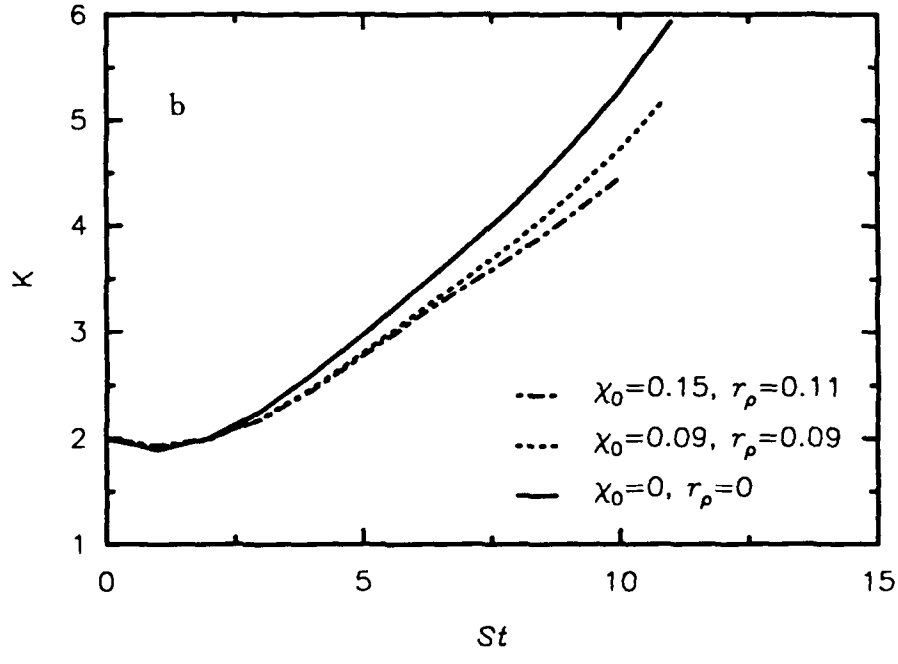

Figure 3 Evolution of kinetic energy for various DNS cases.

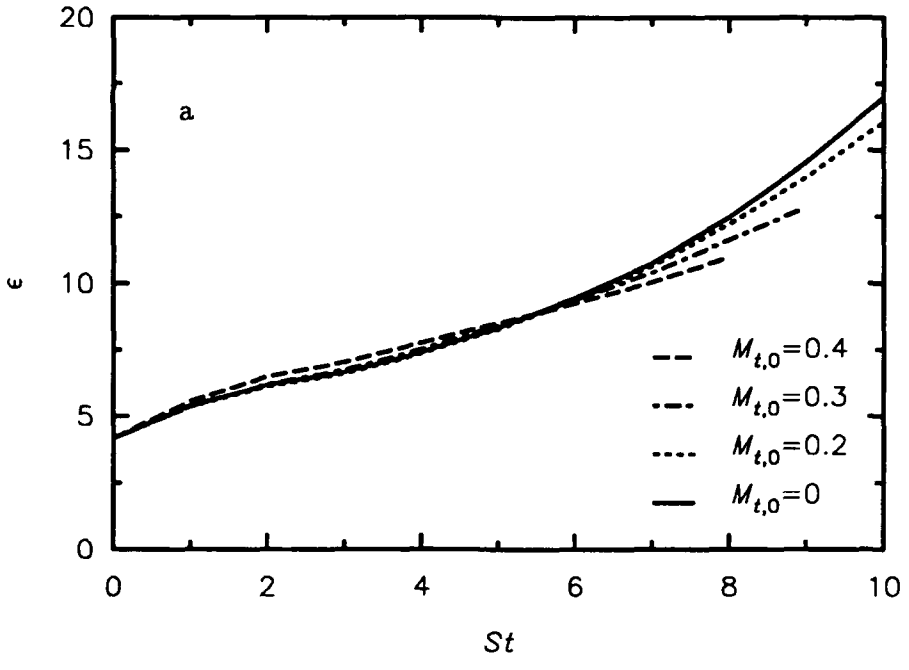

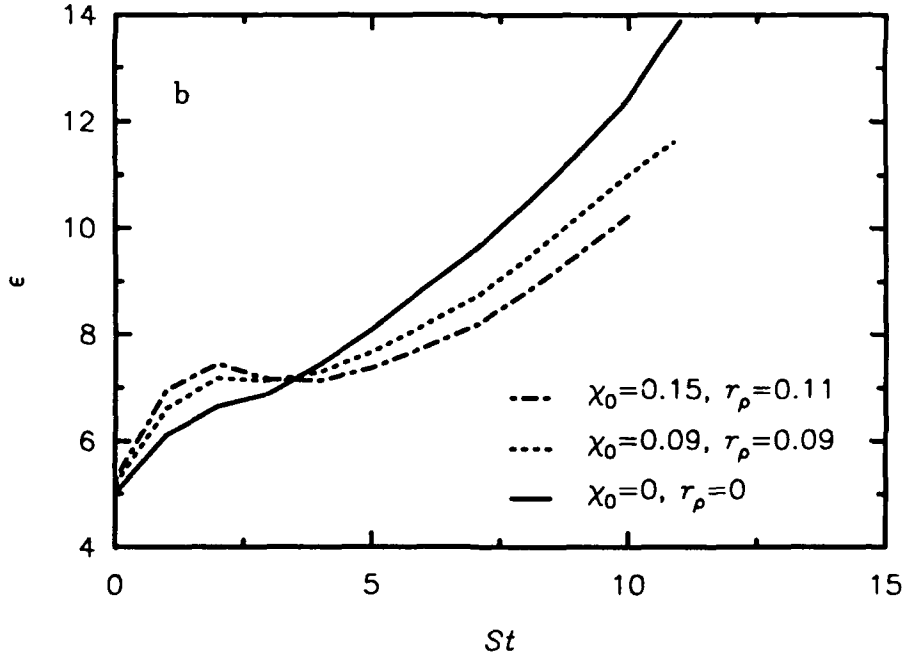

Figure 4 Evolution of dissipation for various DNS cases.

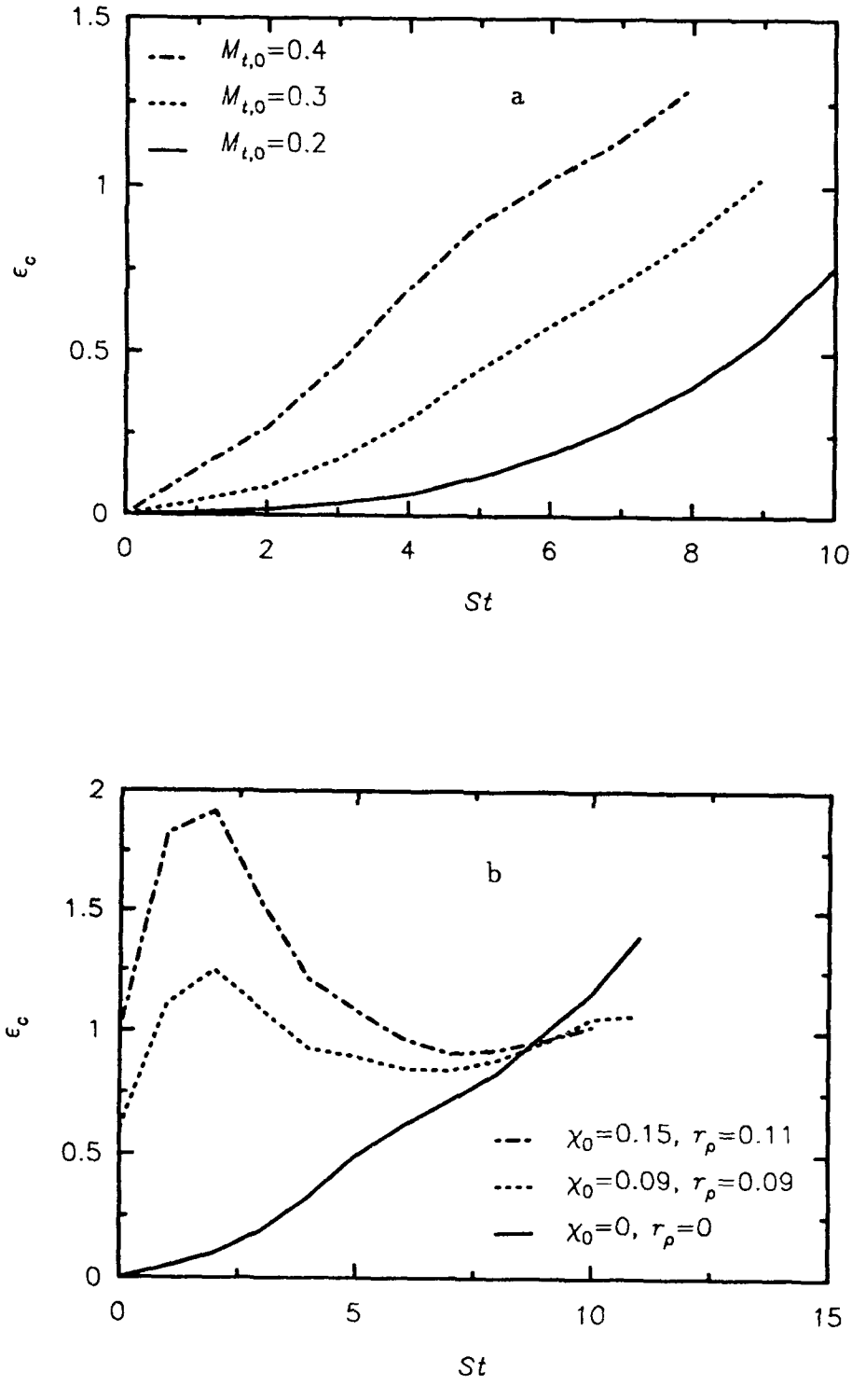

Figure 5 Evolution of compressible dissipation for various DNS cases.

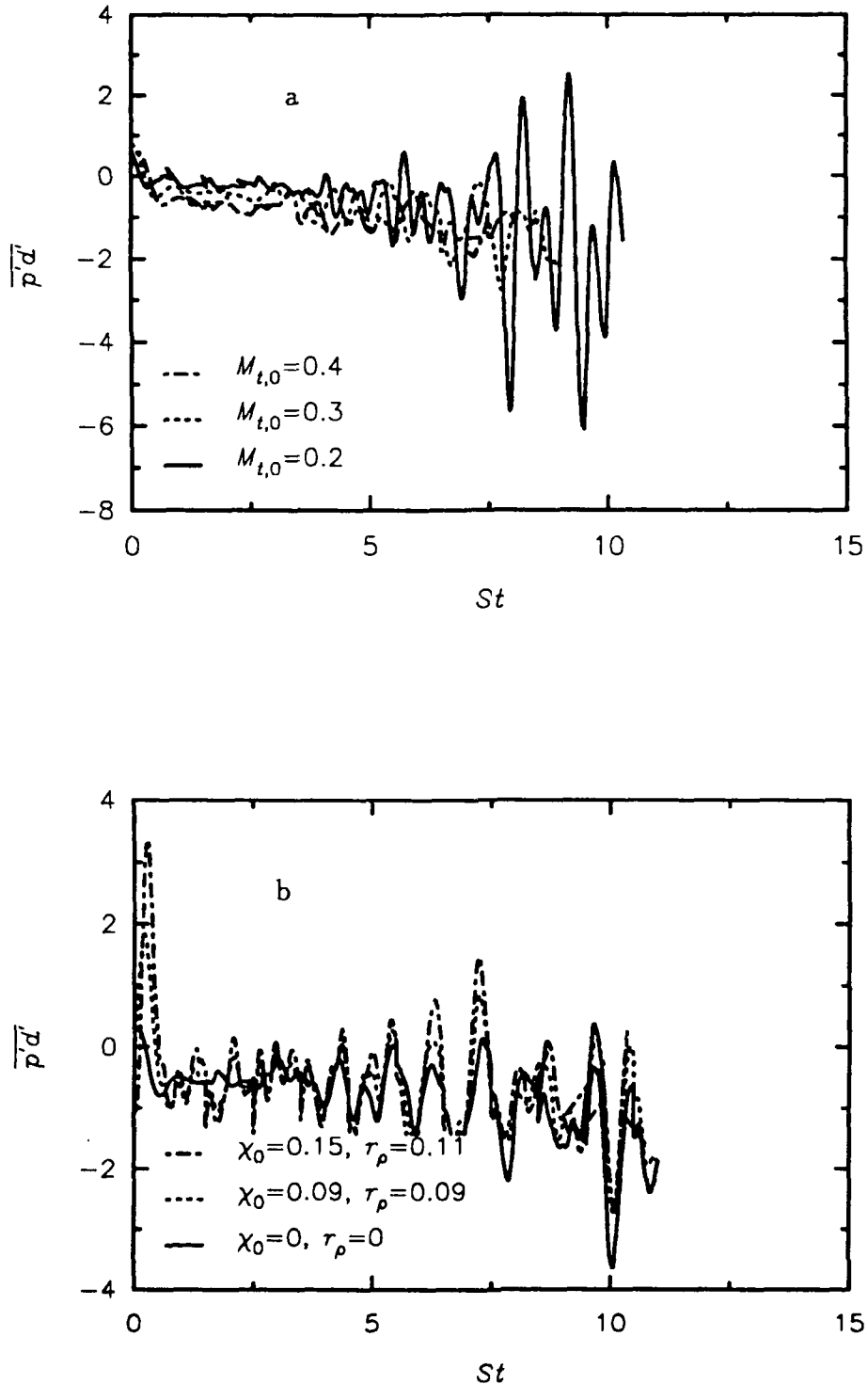

Figure 6 Evolution of pressure-dilatation for various DNS cases

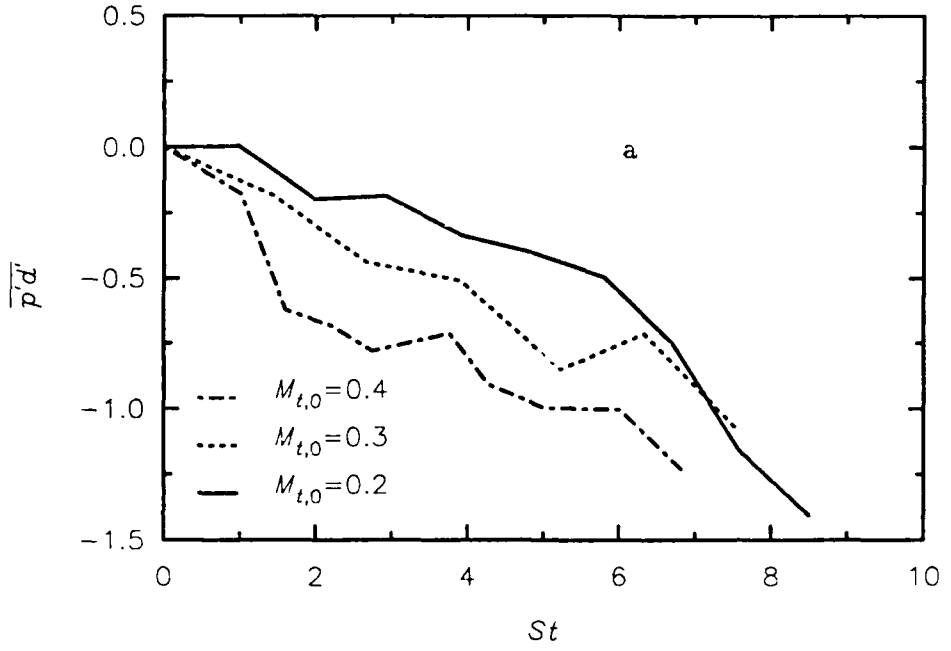

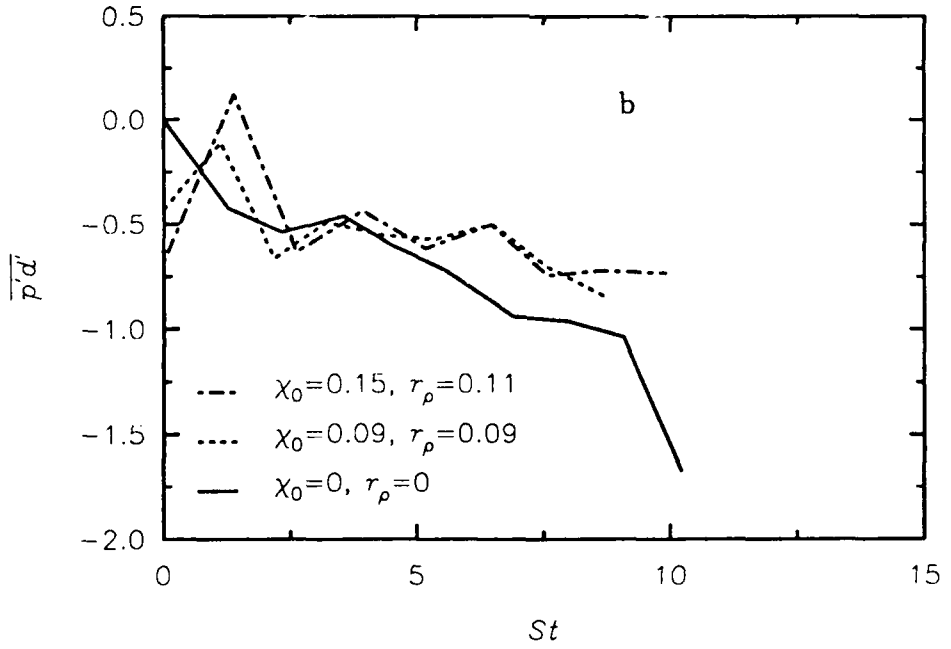

Figure 7 Evolution of time-averaged pressure-dilatation for various DNS cases

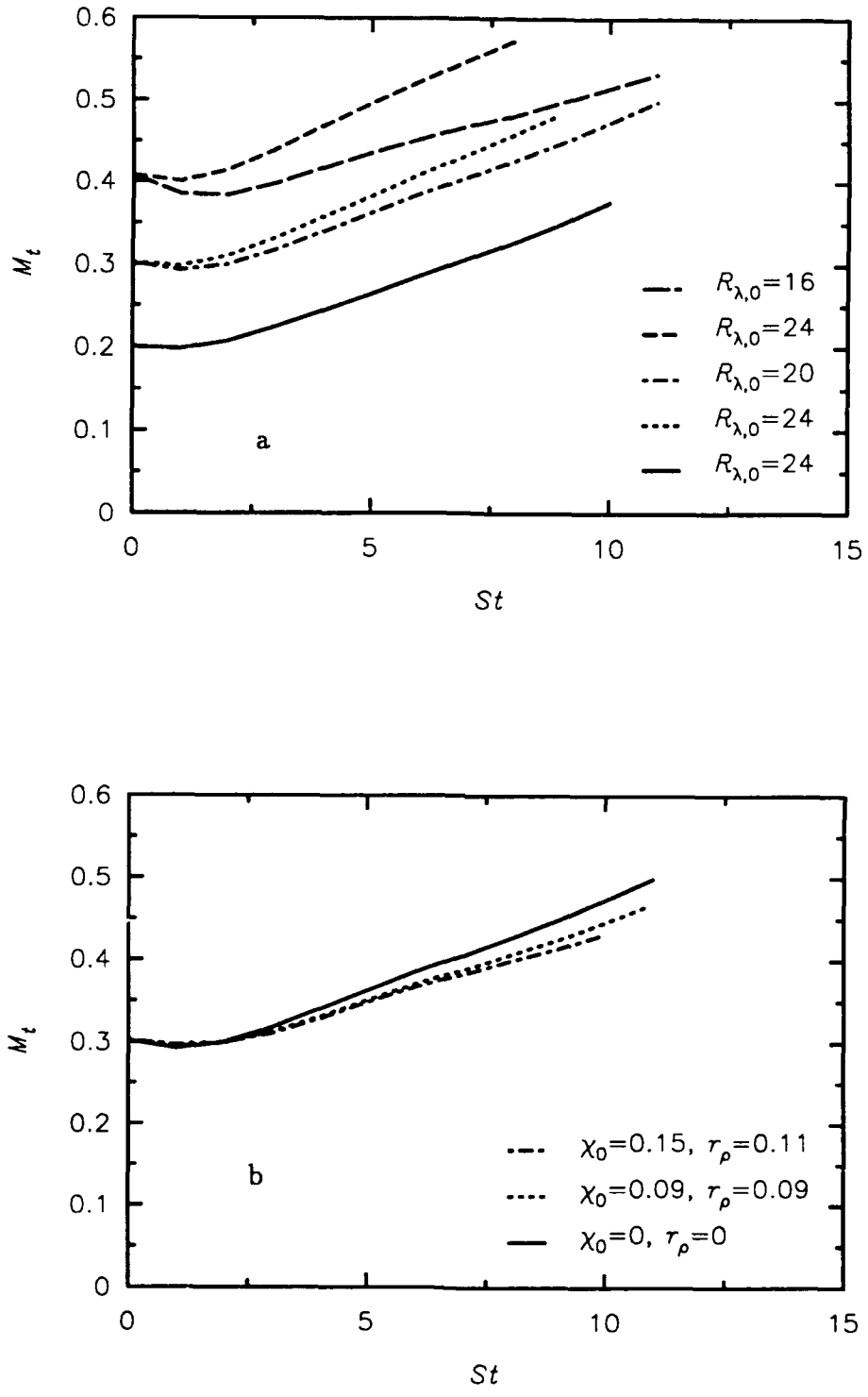

Figure 8 Evolution of turbulent Mach number for various DNS cases.

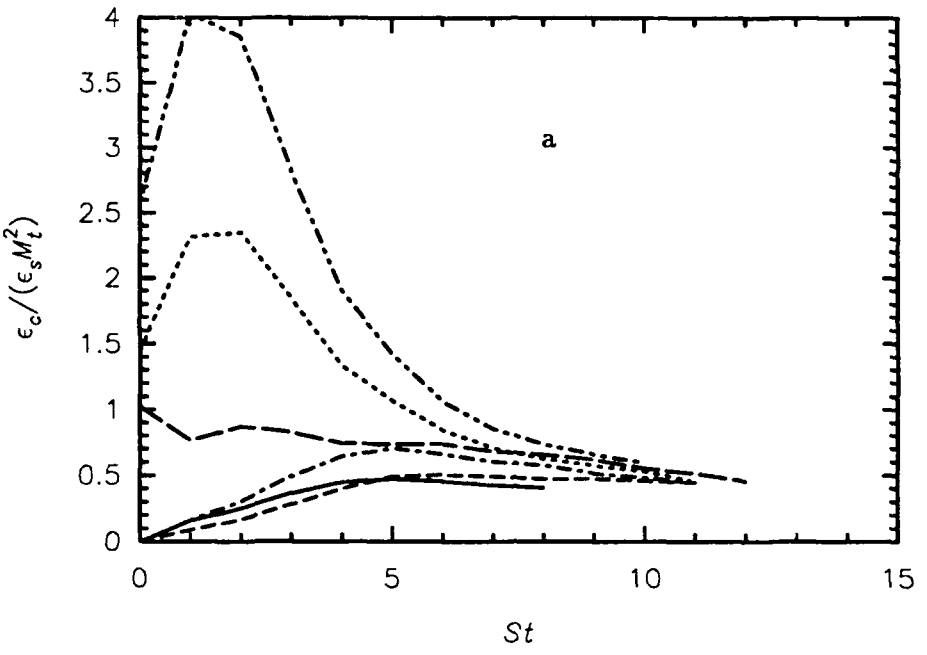

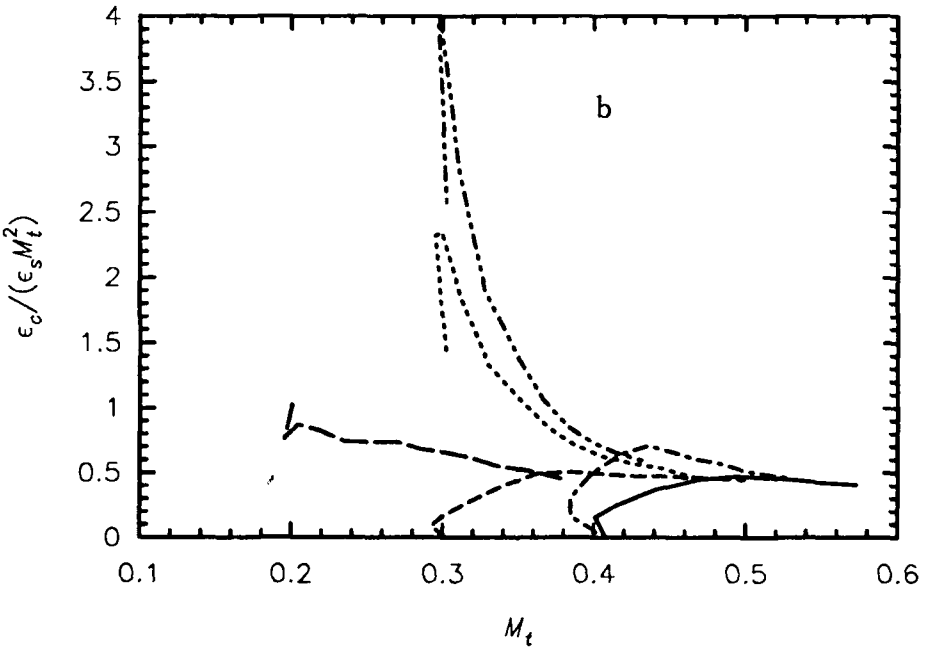

Figure 9 Behavior of scaled compressible dissipation.

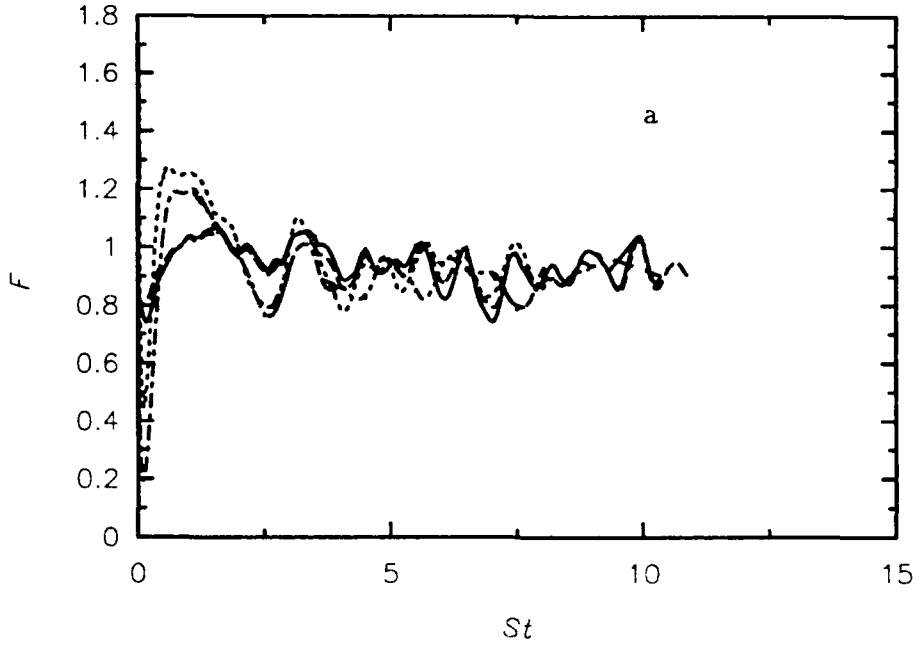

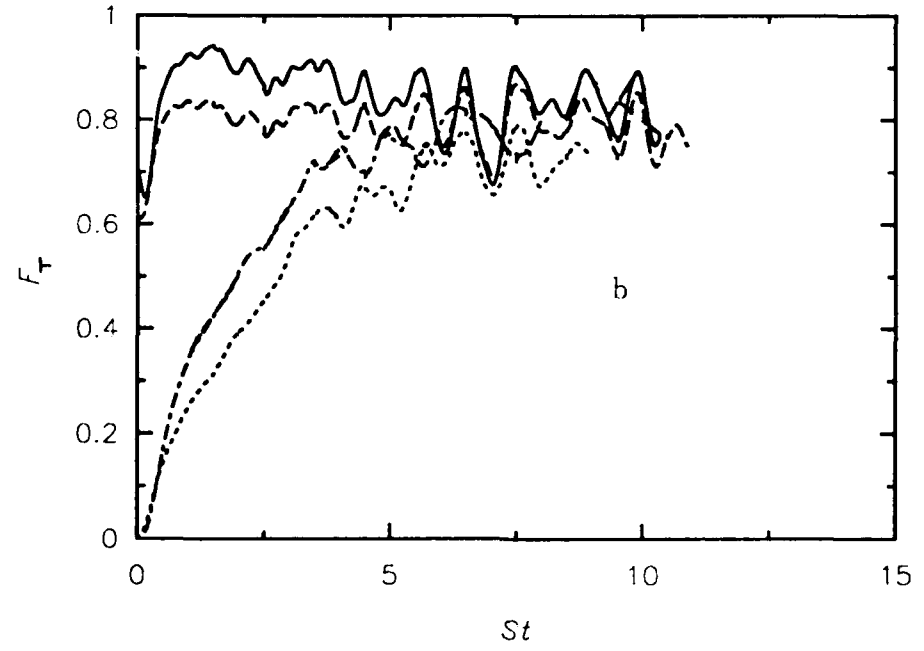

Figure 10 Behavior of the partition parameters F and F_T.

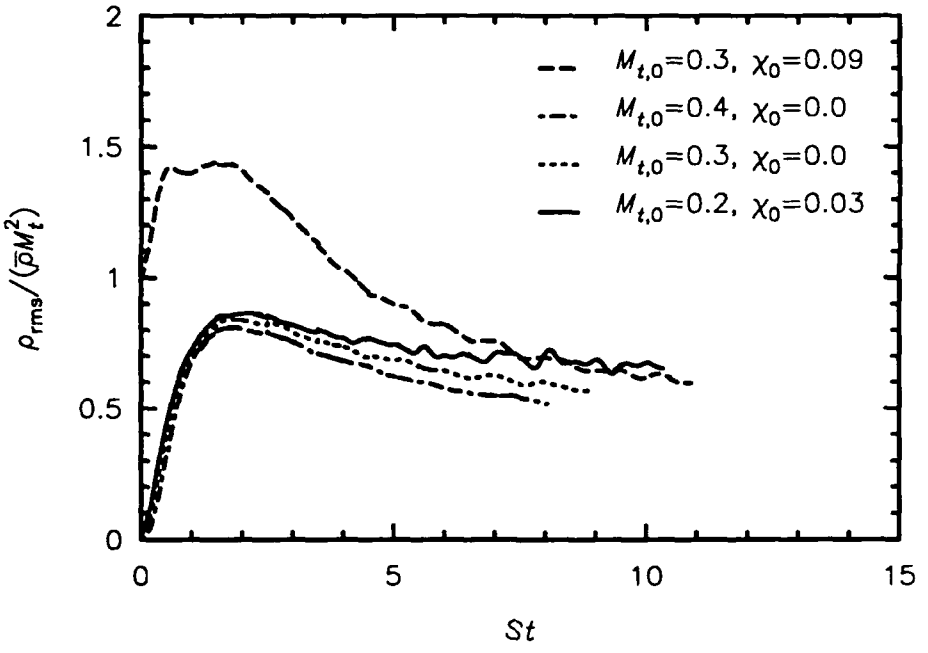

Figure 11a Behavior of scaled rms density.

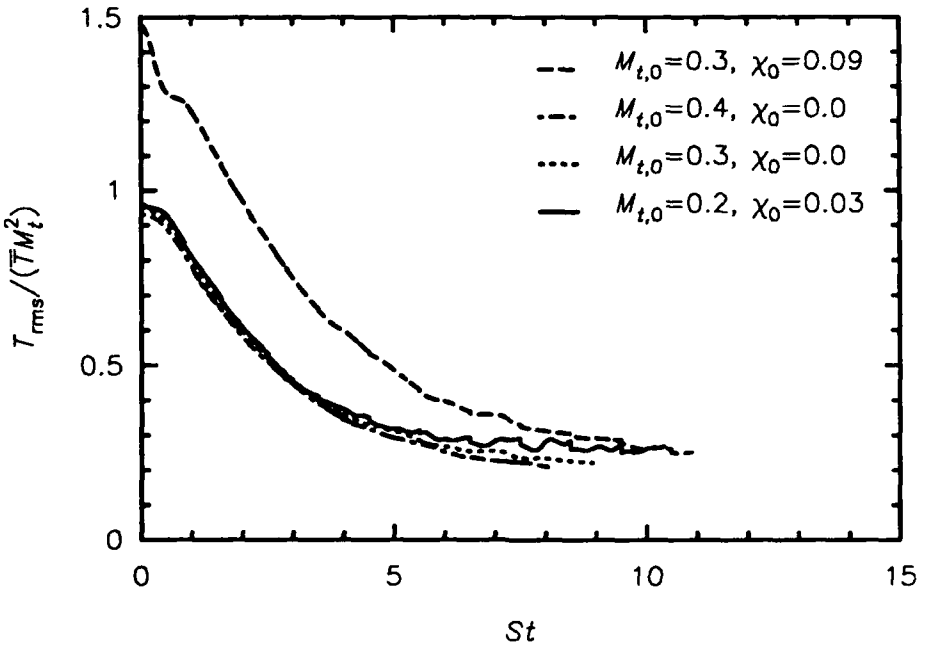

Figure 11b Behavior of scaled rms temperature.

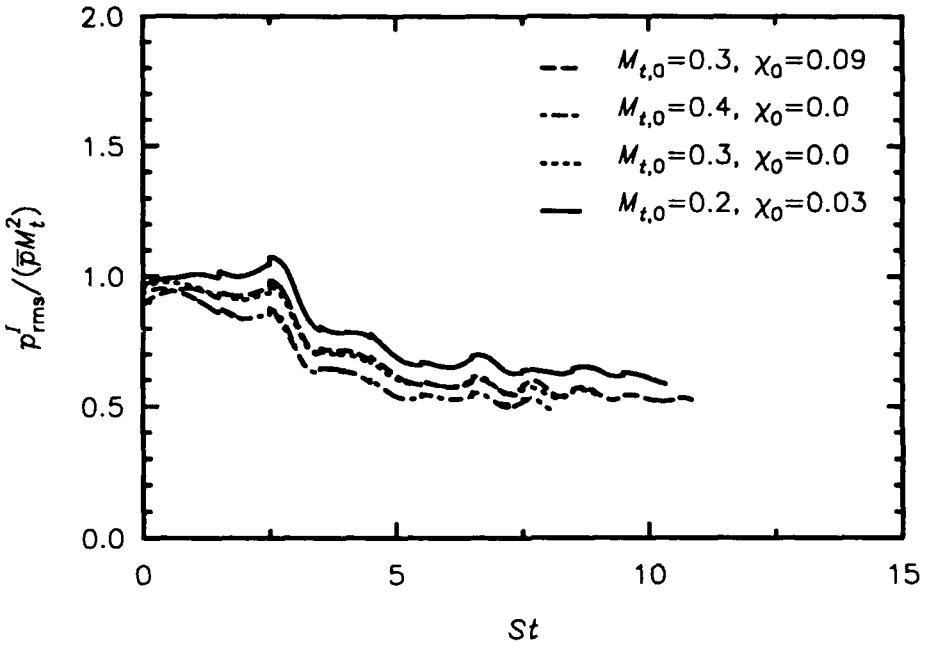

Figure 12a Behavior of scaled rms incompressible pressure.

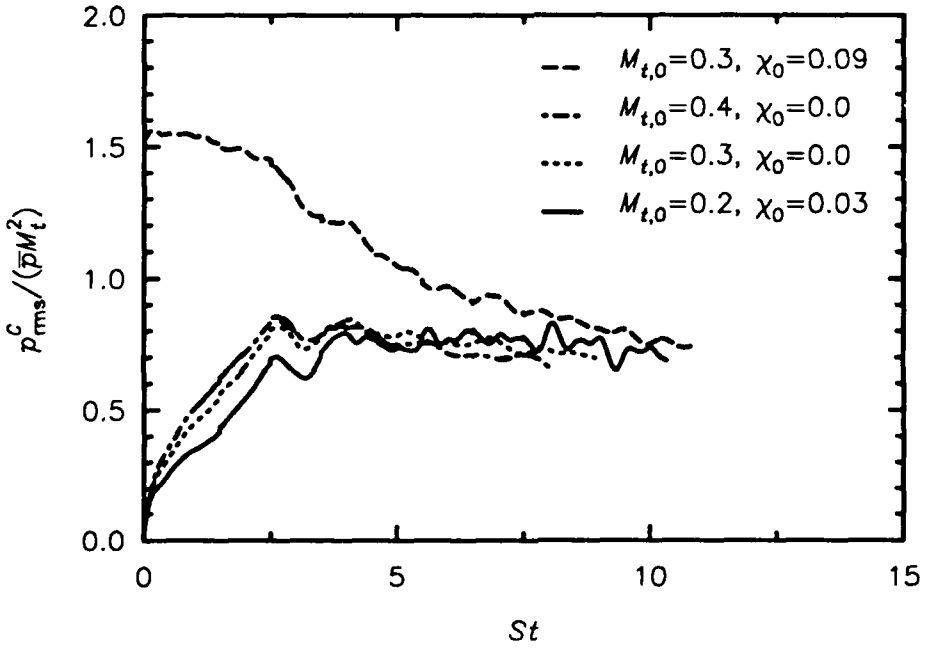

Figure 12b Behavior of scaled rms compressible pressure.

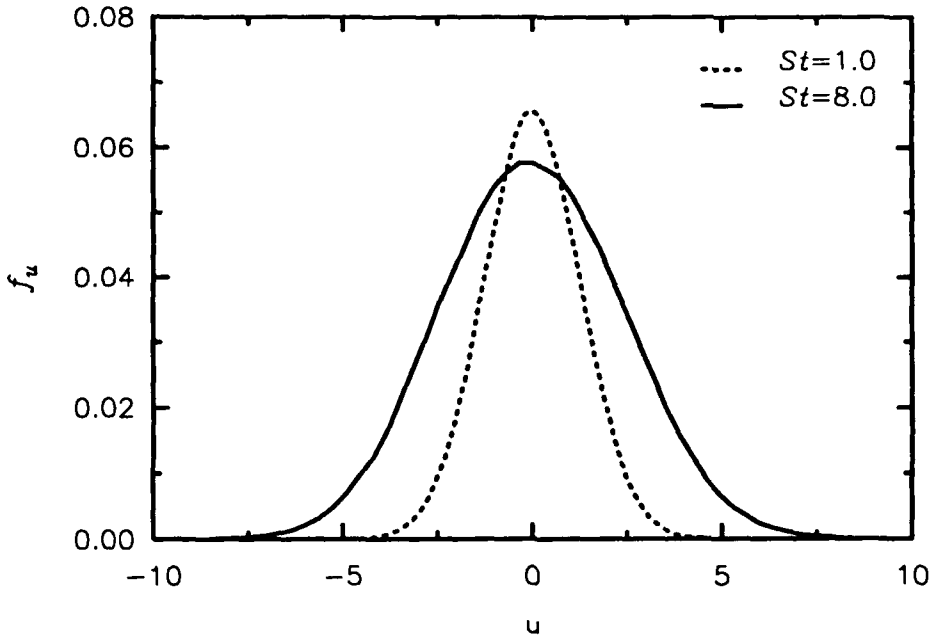

Figure 13a Pdf of streamwise velocity.

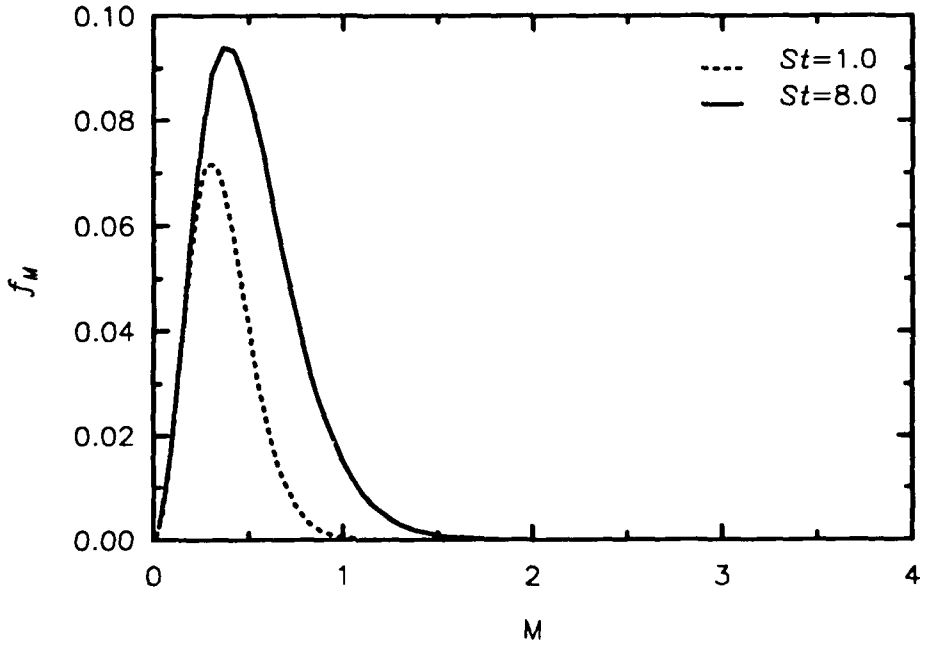

Figure 13b Pdf of Mach number.

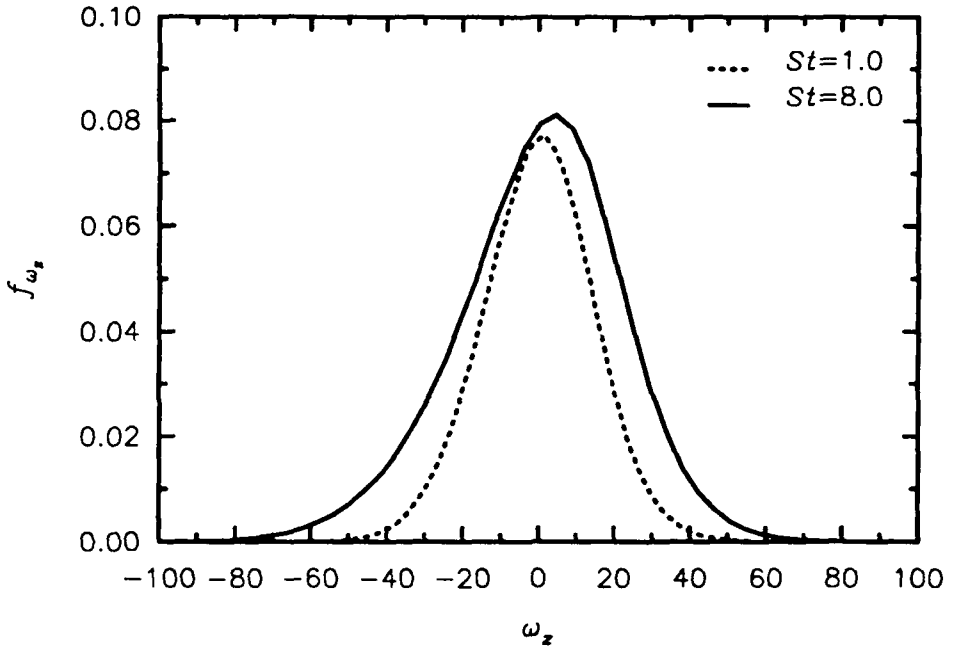

Figure 14a Pdf of spanwise vorticity component.

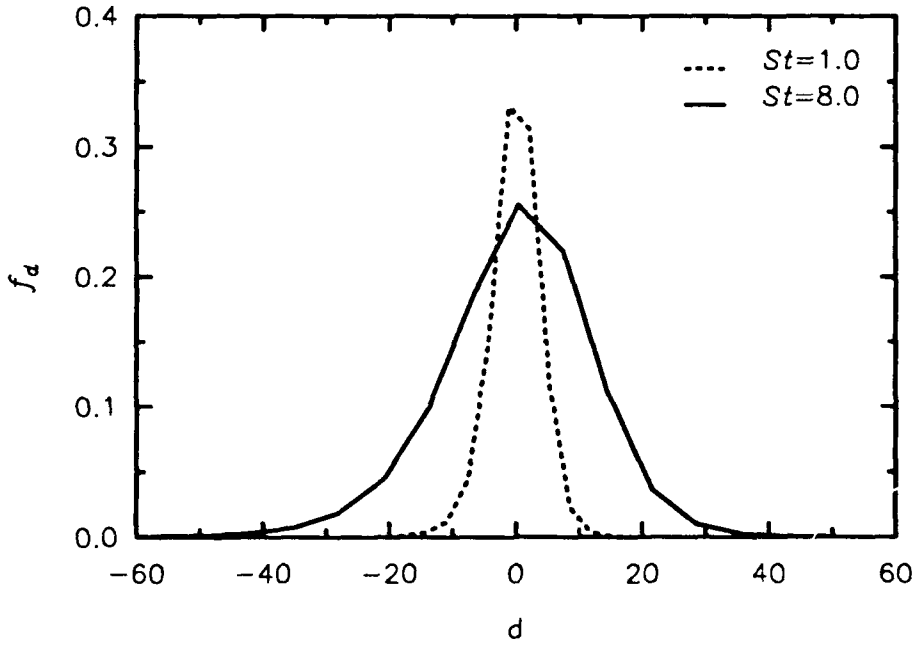

Figure 14b Pdf of dilatation.

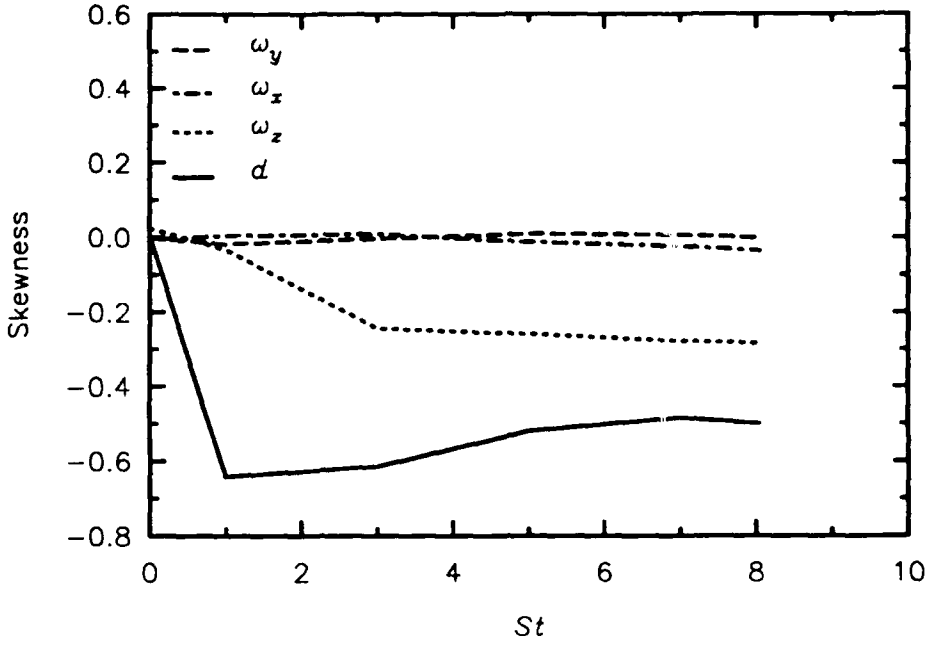

Figure 15a Skewness of vorticity components and dilatation.

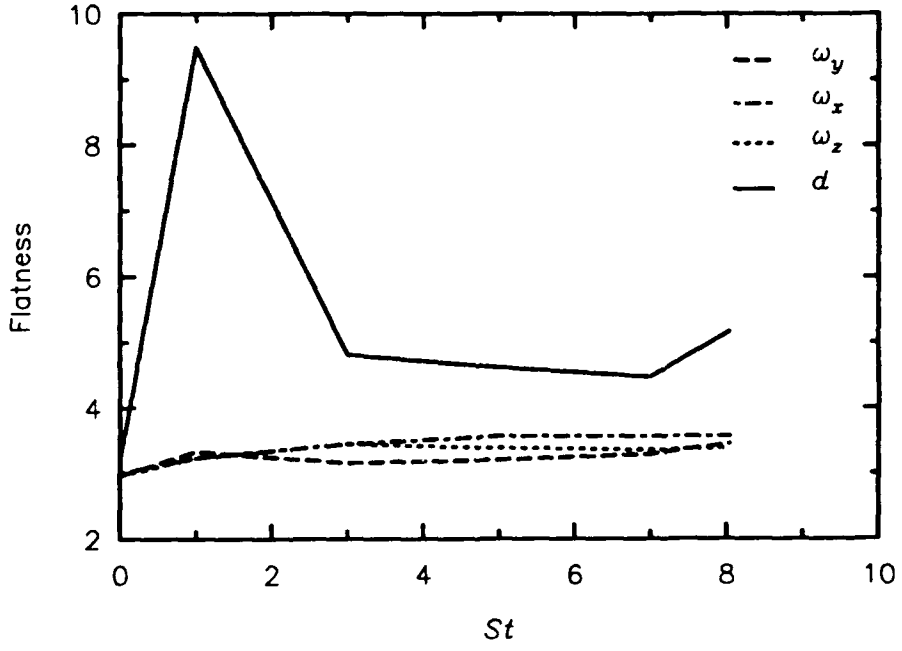

Figure 15b Flatness of vorticity components and dilatation.

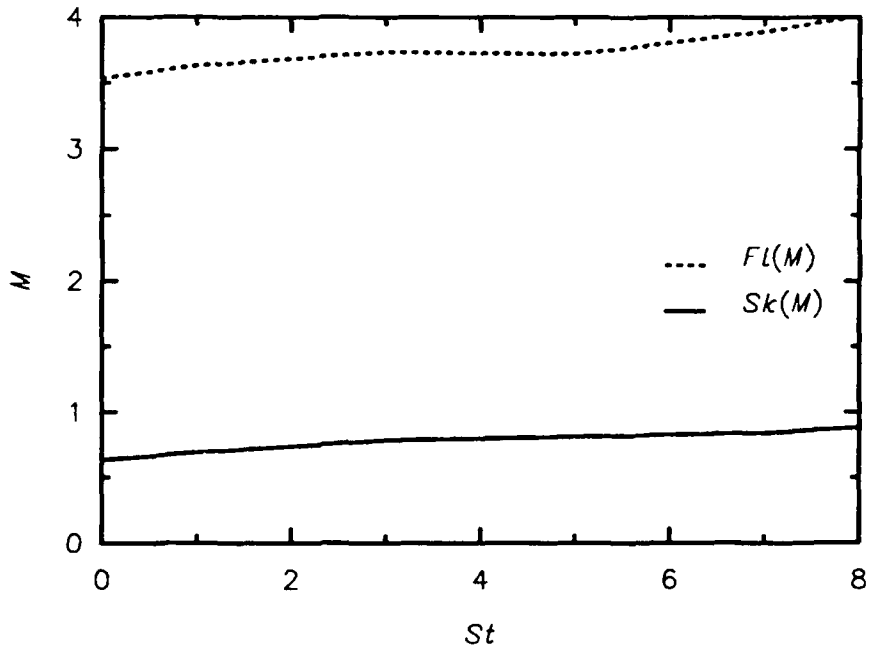

Figure 16a Skewness and flatness of Mach number.

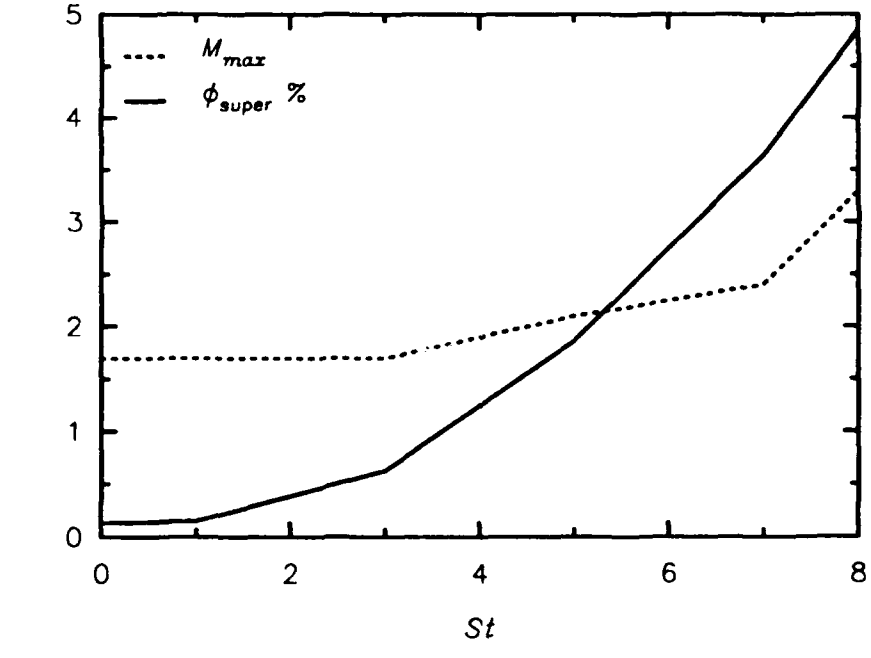

Figure 16b Maximum Mach number and volume fraction of supersonic fluctuations.

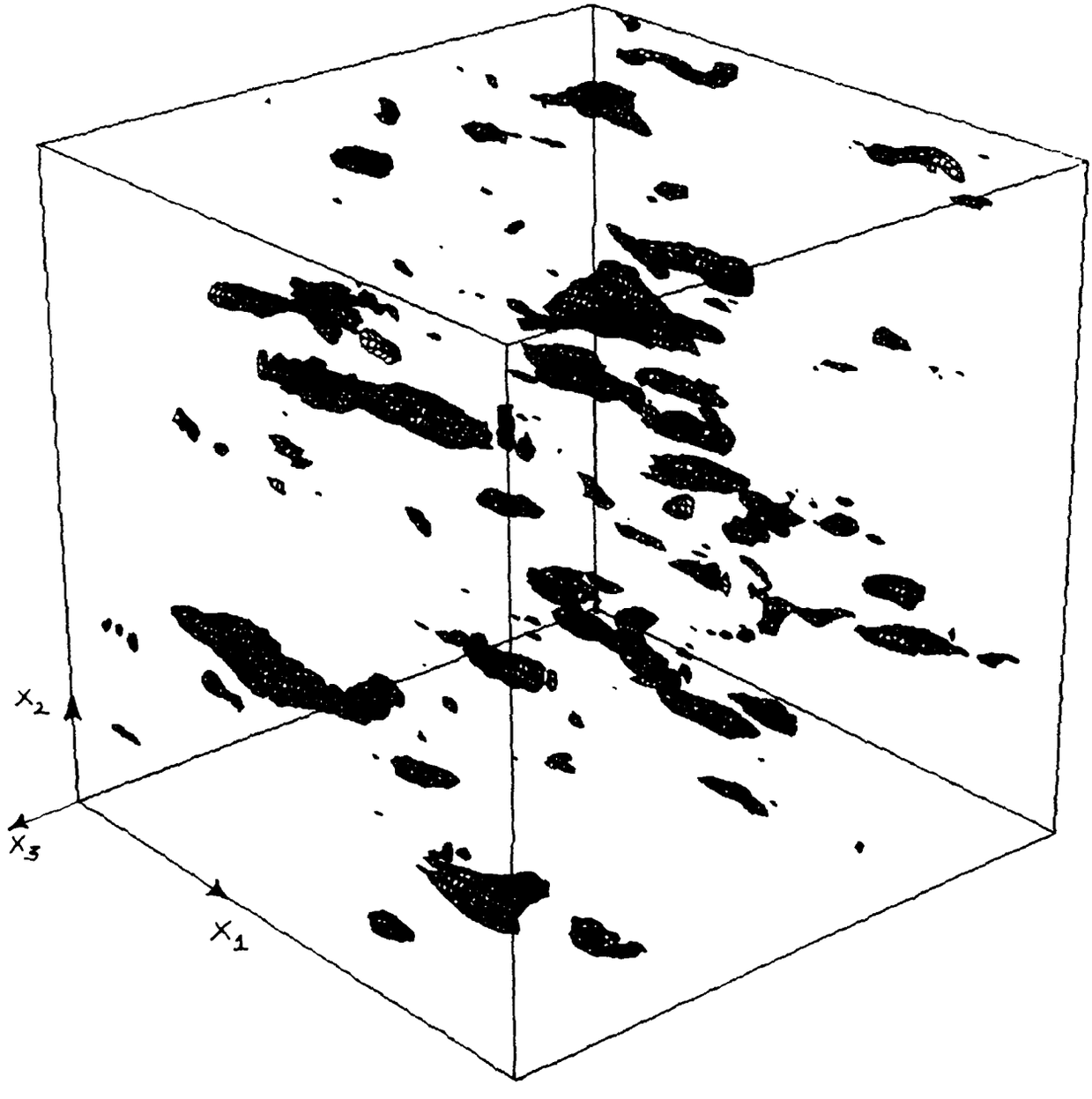

Figure 17 Perspective of supersonic regions in the flow.

Figure 18 Dilatation field in a (x_1, x_2) cut of the flow domain.

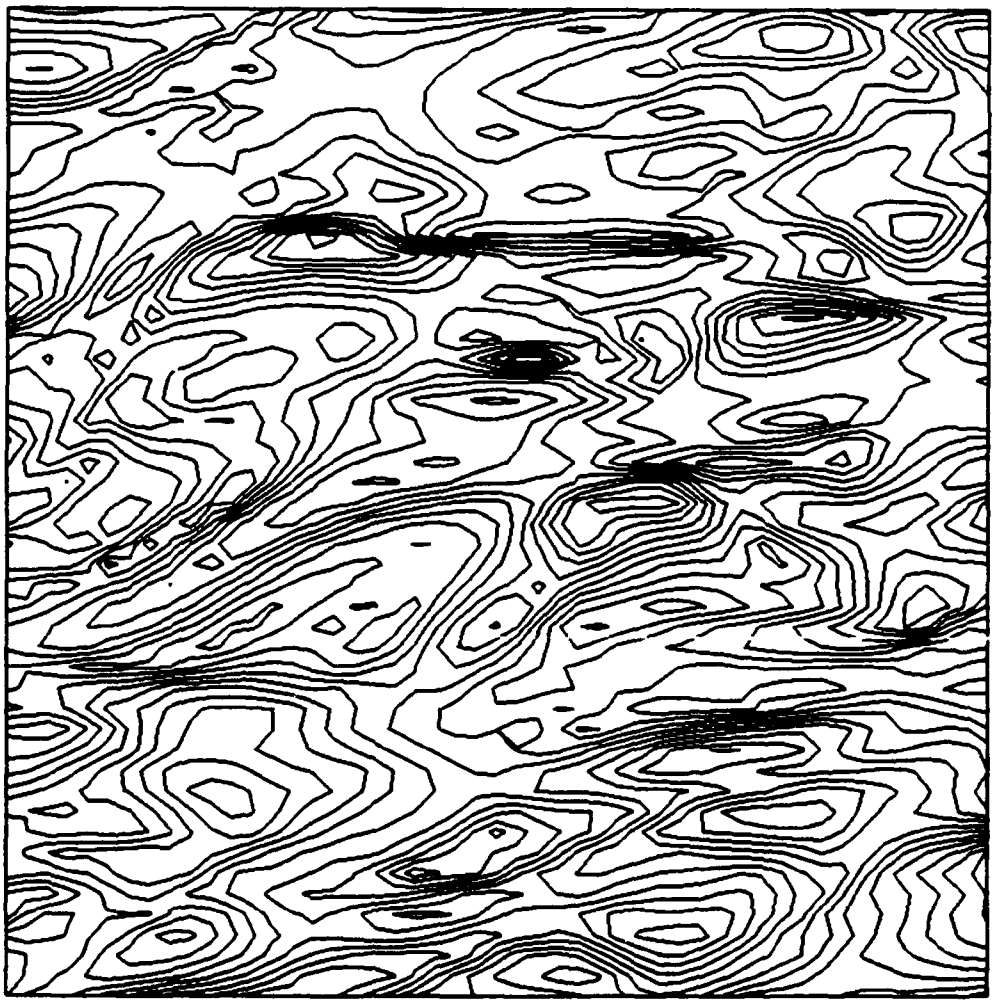

Figure 19a Contours of the magnitude of $u_i^{I'}$ in a (x_1, x_2) cut of the flow domain.

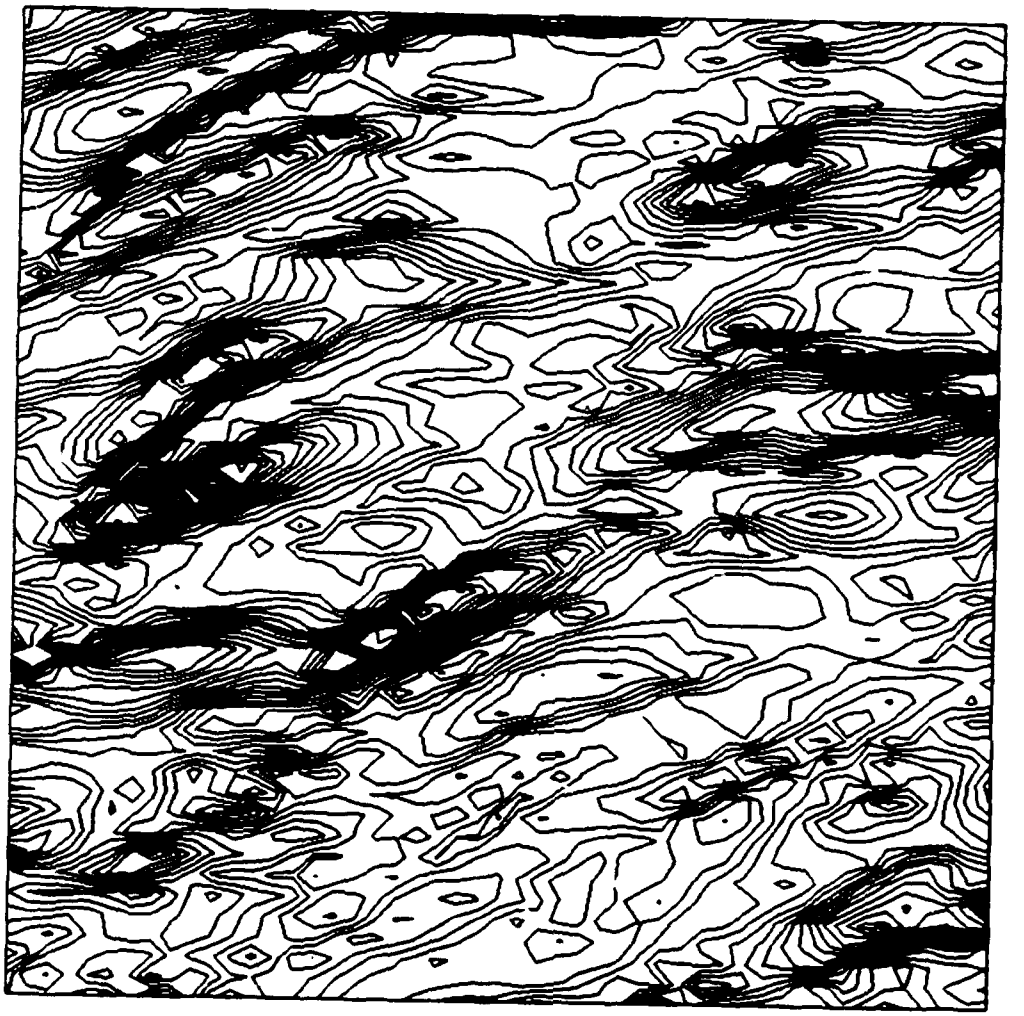

Figure 19b Contours of the magnitude of $u_i^{C'}$ in the plane shown in Fig. 19a.

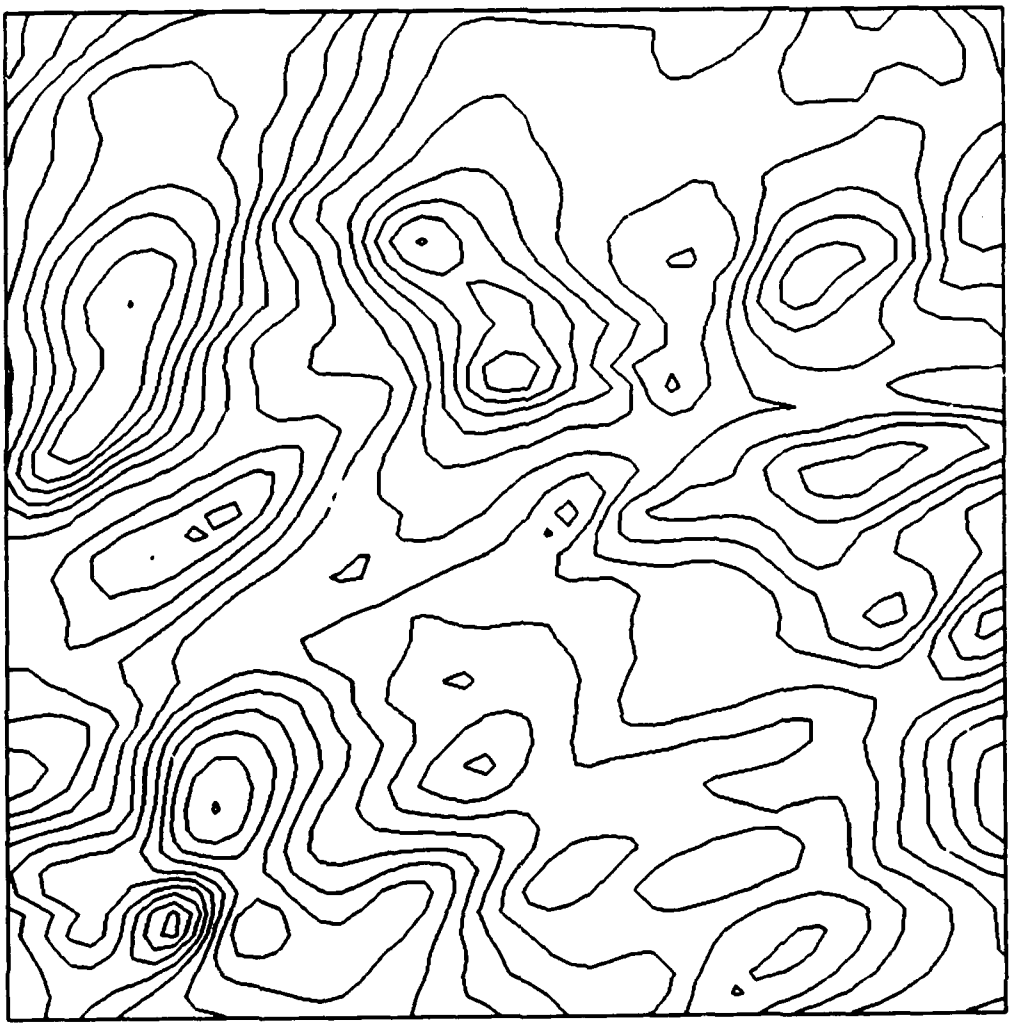

Figure 20a Contours of $p^{I'}$ in the plane shown in Fig. 19a.

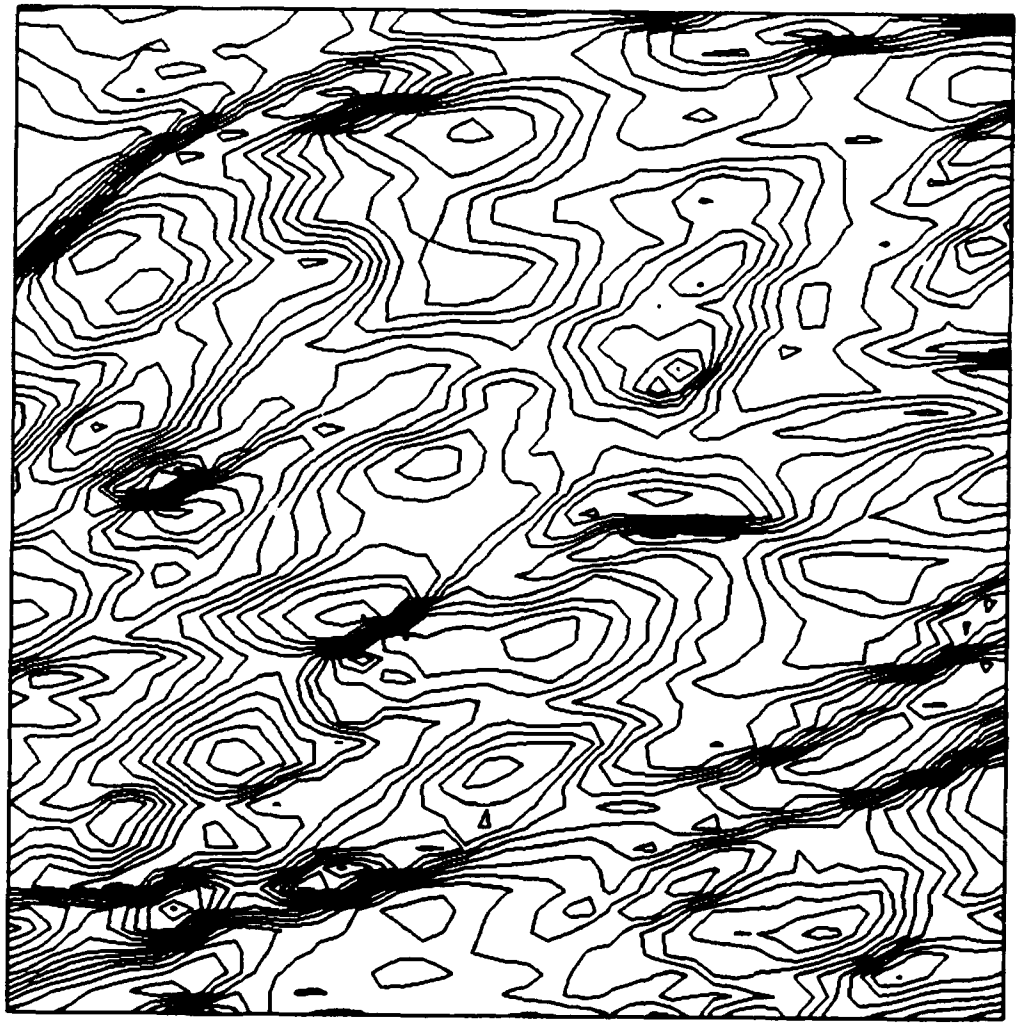

Figure 20b Contours of $p^{C'}$ in the plane shown in Fig. 19a.

Report Documentation Page

1. Report No.	2. Government Accession No.	3. Recipient's Catalog No.
NASA CR-187537 ICASE Report No. 91-29		

4. Title and Subtitle	5. Report Date
DIRECT SIMULATION OF COMPRESSIBLE TURBULENCE IN A SHEAR FLOW	March 1991
	6. Performing Organization Code

7. Author(s)	8. Performing Organization Report No.
S. Sarkar G. Erlebacher M. Y. Hussaini	91-29
	10. Work Unit No.
	505-90-52-01

9. Performing Organization Name and Address	11. Contract or Grant No.
Institute for Computer Applications in Science and Engineering Mail Stop 132C, NASA Langley Research Center Hampton, VA 23665-5225	NAS1-18605
	13. Type of Report and Period Covered
	Contractor Report

12. Sponsoring Agency Name and Address	14. Sponsoring Agency Code
National Aeronautics and Space Administration Langley Research Center Hampton, VA 23665-5225	

15. Supplementary Notes

Langley Technical Monitor:
Michael F. Card

Submitted to Theoretical and Computational Fluid Dynamics.

Final Report

16. Abstract

The purpose of this study is to investigate compressibility effects on the turbulence in homogeneous shear flow. We find that the growth of the turbulent kinetic energy decreases with increasing Mach number - a phenomenon which is similar to the reduction of turbulent velocity intensities observed in experiments on supersonic free shear layers. An examination of the turbulent energy budget shows that both the compressible dissipation and the pressure-dilatation contribute to the decrease in the growth of kinetic energy. The pressure-dilatation is predominantly negative in homogeneous shear flow, in contrast to its predominantly positive behavior in isotropic turbulence. The different signs of the pressure-dilatation are explained by theoretical consideration of the equations for the pressure variance and density variance. We obtained previously the following results for isotropic turbulence; first, the normalized compressible dissipation is of $O(M_t^2)$, and second, there is approximate equipartition between the kinetic and potential energies associated with the fluctuating compressible mode. Both these results have now been substantiated in the case of homogeneous shear. The dilatation field is significantly more skewed and intermittent than the vorticity field. Stong compressions seem to be more likely than strong expansions.

17 Key Words (Suggested by Author(s))	18. Distribution Statement
turbulence, compressible fluids, direct numerical simulations	02 - Aerodynamics Unclassified - Unlimited

19 Security Classif. (of this report)	20. Security Classif. (of this page)	21 No. of pages	22 Price
Unclassified	Unclassified	41	A03

NASA FORM 1626 OCT 86